NASA CR - 54084

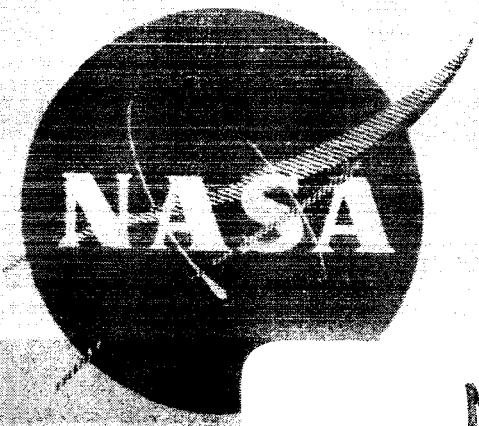

Research and Development of High-Performance Light-Weight Fuel Cell Electrodes

SECOND QUARTERLY REPORT

FEBRUARY 1 - APRIL 30, 1964

by

R. G. Holdeman, Principal Investigator

W. A. Barber
W. P. Colman

prepared for

NATIONAL AERONAUTICS AND SPACE ADMINISTRATION

CONTRACT NAS 3-2786

AMERICAN CYANAMID COMPANY

CYANAMID

NASA CR-54084

SECOND QUARTERLY REPORT

RESEARCH AND DEVELOPMENT OF HIGH-PERFORMANCE LIGHT-WEIGHT FUEL CELL ELECTRODES

by

R. G. Haldeman, Principal Investigator
W. A. Barber
W. P. Colman

prepared for

NATIONAL AERONAUTICS AND SPACE ADMINISTRATION

June 29, 1964

CONTRACT NAS 3-2786

Period Covered: February 1, 1964 - April 30, 1964

NASA Lewis Research Center
Cleveland, Ohio
Space Power Systems Division
Technical Manager: Mr. W. A. Robertson MS-86-1

AMERICAN CYANAMID COMPANY
STAMFORD RESEARCH LABORATORIES
1937 West Main Street
Stamford, Connecticut
(Area Code 203) 348-7331

ABSTRACT

24995

The overall object of this contract is the reduction of the weight-to-power ratio of the hydrogen-oxygen fuel cell. Work in the second quarter of the contract has been concentrated on (1) materials studies including catalysts, supports and matrices, (2) modification of thin platinum/screen type electrodes, (3) evaluation of cell operating variables, (4) life-testing of standard electrodes, and (5) engineering analysis of cell scale-up.

Catalyst studies included sintering of high area platinum blacks and evaluation of palladium containing electrodes. Asbestos-poly(vinyl alcohol) continues to show promise as an electrolyte matrix. Electrode variables included platinum loading, Teflon content, and expanded metal supports. Improved life performance of Cyanamid standard electrodes was demonstrated. Preliminary analysis was made of methods of heat and water removal in a 2 kilowatt battery. System weights (not including tankage) of 50-100 lbs/kw appear feasible.

AUTHOR

TABLE OF CONTENTS

TABLE OF CONTENTS

(Continued)

LIST OF TABLES

LIST OF FIGURES

1. INTRODUCTION

1.1 Objectives

The objectives of the National Aeronautics and Space Administration Contract NAS 3-2786 are indicated by Article I in the Statement of Work of RFP No. APGO-1508.

ARTICLE I - OBJECTIVES

(a) A fuel cell utilizing hydrogen and oxygen reactants is of considerable interest to NASA because of its high electrical work output per unit of weight of reactants. The efficiency of hydrogen-oxygen fuel cells is 60% or better in practical cells. These cells have a power plant weight of approximately 150 pounds per kilowatt neglecting reactants and tankage. The chief objective of hydrogen-oxygen fuel cell research is the reduction of the weight-to-power ratio.

(b) An important factor in determining the fuel cell weight is the weight of the electrode and its supporting structure. The intent is to support research and development efforts directed towards obtaining electrode systems which will produce a higher electrochemical reaction rate per unit weight of electrode and assembly while maintaining a satisfactory fuel consumption efficiency.

(c) While this RFP suggests that high-performance, light-weight electrodes are the basic interest, it should be understood that the weight and efficiency of the entire power plant must be included to in fact achieve the purpose of this effort: namely, the reduction of the fuel cell weight-to-power ratio.

1.2 Scope

The scope of work to be done by American Cyanamid Company during the contract year is outlined in the Schedule of Work, presented in the First Quarterly Report.

Work in the second quarter of the contract was devoted primarily to Phase I of the Schedule of Work. Emphasis was given particularly to (1) materials, including catalysts, supports, and matrices, (2) study of modifications of American Cyanamid Type A and Type B electrodes, and (3) the development of suitable small test vehicles for evaluation of both initial and life performance of the above electrodes. Initial engineering analysis was made for Phase II, which deals with scale up of single cells to approximate battery dimensions and configuration. Plans for work in the third quarter of this contract are included in the last section of this report.

2. SUMMARY

Following is a summary of the major findings of the second quarterly report period.

(1) Further work with high area platinum blacks indicated that a major portion of the platinum surface area was lost in the electrode manufacturing process. In contrast, standard platinum black lost relatively little surface area during electrode preparation.

(2) Although exposure of both commercial and high area platinum blacks alternately to air and hydrogen caused severe sintering of the powders, similar treatment of the formed electrodes produced very little further change in platinum surface area.

(3) The use of both commercial and laboratory catalyst preparations containing palladium in Type A electrodes was investigated. It was found that at standard loadings (9 mg/cm^2) or higher, performance of palladium-containing catalyst was poorer, or at best equivalent, to the same loading of commercial platinum black. With Type B electrodes (catalyst supported on carbon) at catalyst loadings of 1 to 2 mg/cm^2, and when used as cathode, a small performance advantage was obtained with palladium over platinum. However, performance was well below that of standard electrodes.

(4) Since the several catalyst studies to date indicated no significant advantages over commercial platinum black, it is planned to use the latter material exclusively in the further electrode development performed under this contract.

(5) It was shown that at 70°C electrodes containing 40 mg Pt/cm^2 and 25% Teflon (based on platinum-Teflon content) supported on 40 mesh nickel screen produced a 20 millivolt increase in cell working potential over the current density range 40 to 400 ma/cm^2. Thus, at 400 ma/cm^2 cell potential was about 0.80 volt.

(6) Studies of the effect of increased loading at anode and cathode indicated that at low current densities improvement was associated with higher loading at the oxygen electrode. At high current densities improvement was associated with higher loadings at the hydrogen electrode.

(7) No apparent advantage was found for graded waterproofing of electrodes.

(8) No advantage in electrode performance was found in the use of expanded nickel over nickel screen in the electrode structure.

(9) An improved 2" x 2" test cell utilizing Teflon gasket and matrix seal was developed and adopted as standard for life-testing.

(10) The effect of electrolyte loading and cell assembly pressure on electrolyte distribution, cell internal resistance, and performance was investigated. For 20 mil Fuel Cell Asbestos, an electrolyte loading of 1.0 - 1.5 g/g dry matrix, and a cell assembly pressure of 120 - 180 p.s.i. is optimum.

(11) The influence of concentration of KOH in the electrolyte on performance stability was investigated at 70°C for four sets of conditions involving standard and high platinum electrodes, and matrices of Fuel Cell Asbestos Board and "ACCO" asbestos. With standard electrodes and Fuel Cell Asbestos Board, operation becomes sensitive to KOH concentration at current densities greater than 200 ma/cm^2. With high-loading electrodes and ACCO asbestos, short term stability can be achieved to at least 800-1000 ma/cm^2 .

(12) Preliminary experiments on the effect of pressure at 70°C indicated that over the current density range 40-200 ma/cm^2 an increase in cell potential of 35-40 millivolts can be achieved by increasing operating pressure from 0 to 20 psig.

(13) The influence of concentration of carbonate in the electrolyte on cell performance was studied. The data show that at 70°C and 100 ma/cm^2, reduction in cell potential amounts to about 30 millivolts when nearly half of the potassium is present as carbonate. Beyond this carbonate level performance drops rapidly.

(14) Improved life performance at 70°C and 100 ma/cm^2 has been achieved with standard electrodes using both dry and presaturated inlet gases. One test has been running for over 1800 hours with a net drop in cell potential from 0.845 to 0.813 volt.

(15) In general it was observed that during life-testing, internal resistance increases slowly as potential falls. It has been found that occasional reversal of gases, e.g., after 500 hours, has a stabilizing effect on both resistance and cell potential.

(16) In preparation for scale-up of experimental cells, consideration has been given to various systems for heat and water removal. Calculations show that in a 2 kilowatt dynamic system, the gas recycle pump is a major weight factor. Operating at high humidities (i.e., high cell temperatures and low electrolyte concentrations) is desirable to minimize the weight of the gas recycle pump. Maintaining both heat and water balances by means of excess gas flow appears impractical because of the very high gas recirculation rates required. Total system weights (battery and auxiliaries, but not reactant tankage) of 50-100 lbs/kw should be attainable with either dynamic or static systems.

3. MATERIALS INVESTIGATION

3.1 Catalysts

Work in the preceding report period[1] indicated that platinum black with a surface area significantly higher than that of commercially available material could be prepared, but no better performance characteristics in a hydrogen-oxygen fuel cell could be achieved. During the present report period this investigation has been extended. Also, an investigation was made of the use of palladium as catalyst in thin electrode structures.

3.1.1 High Area Platinum

A possible explanation of the lack of improvement in performance of electrodes formed from high area platinum black has been uncovered by surface area measurements on the formed electrode discs. Surface area measurements by nitrogen adsorption made on standard platinum black before and after formation into an electrode show a significantly lower platinum surface area in the formed electrode. Thus, as indicated in Table 3-1, a decrease of 10 m^2/g to about 2/3 of the original area was observed in one set of experiments.

There seems to be a considerably larger decrease in surface area in forming electrodes from high area platinum. A series of electrodes was made with an experimental platinum black of specific area 42 m^2/g and with levels of Teflon binder from 5 to 35%. Electrodes made from this black had surface areas of platinum in the range 11 to 19 m^2/g, a reduction to 1/4 to 1/2 of the original area. Indeed, the latter surface areas were substantially below that found for standard electrodes. Performance of these electrodes was in no case better than standard. It is obvious that the high surface area platinum is more sensitive than commercial black to the process of making electrodes. In view of this result, no additional work on high area platinum is contemplated.

TABLE 3-1

Platinum Surface Area Before and After Electrode Formation

Pt Black No.	Prior Treatment	Pt Surface Area, m^2/g Powder	Electrode
Commercial	None	30	21
	After H_2 treatment		20
	Second H_2 treatment		19
49	None (5% Teflon)	42	11
	After H_2 treatment		11
	None (10% Teflon)	42	10
	After H_2 treatment		11
	None (20% Teflon)	42	11
	After H_2 treatment		12
	None (35% Teflon)	42	19
	After H_2 treatment		16

In our previous report we described the extensive sintering of both commercial and high area platinum black powders when initially exposed to air, purged with nitrogen, and then exposed to hydrogen at ambient temperature. The data in Table 3-1 show that once the platinum black is formed into an electrode on a metal screen, it is relatively free of surface area change; even on repeated alternate exposure to air and hydrogen.

3.1.2 Palladium Catalysts

It is well known that palladium is a catalyst of activity similar to platinum when used in alkaline electrolyte fuel cells. Therefore, it seemed useful to examine the performance of palladium in the thin electrode structures presently under investigation. Both commercial palladium black (surface area 19 m^2/g) and laboratory samples (prepared by the methods described previously for platinum black[1]) were examined.

Initially it was thought that a high area palladium or perhaps a codeposited mixed black of platinum-palladium might give increased performance, in accordance with the objectives of this contract. Unfortunately, efforts to prepare high area blacks containing palladium have been unsuccessful so far, since, in general, surface areas of laboratory samples have fallen in the range of 10-15 m^2/g.

Electrodes were made of a number of these materials and some representative performance data are shown in Table 3-2. These data were obtained in cells using standard AB-1 counter electrodes. Data for lower levels of platinum and palladium deposited on carbon are also included.

TABLE 3-2

Evaluation of Electrodes Containing Palladium

vs. Standard Counter Electrode

1" Diameter Cell; 5N KOH; Filter Paper Matrix

Anode: / Cathode: / Temperature: / Current Density, ma/cm²		Cell Working Potential, Volts							
		Test Electrode / Standard AB-1				Standard AB-1 / Test Electrode			
		25°C		70°C		25°C		70°C	
		40	180	40	180	40	180	40	180
Electrode	Catalyst, mg/cm²								
Commercial	9 Pt	.92	.80	.93	.84	.92	.80	.93	.84
Commercial	20 Pd	.87	.75	.93	.83			.93	.84
94-2	20 Pd	.85	.64	.92	.83			.93	.84
93-3	16 Pd + 4 Pt	.91	.76	.93	.83				
94-1	14 Pd + 6 Pt	.91	.79	.93	.84				
168-3	10 Pd	.86	.73			.88	.79		
79-3	7.5 Pd + 2.5 Pt	.89	.70			.87	.73		
9-2	6 Pd + 2 Pt + 2 Rh	.90	.64	.92	.78				
Supported on Carbon									
X-1	2.0 Pt	.85	.69			.86	.71		
160-3	2.0 Pd	.81	.66			.88	.75	.88	.78
64-2	1.5 Pd + 0.5 Pt	.86	.68			.86	.71		
	1.0 Pt	.83	.66			.81	.68		
180-3	1.0 Pd	.77	.57			.82	.71		

Mixtures of metals were prepared by coprecipitation. For reference, data on electrodes prepared from commercial platinum and palladium blacks are shown.

In our experience, all palladium catalysts are equal to or inferior to the same quantity of platinum when used at the hydrogen electrode. At the oxygen electrode, we have found that at lower levels of catalytic metal (1 or 2 mg/cm^2) palladium performs slightly better than the same quantity of platinum. This difference is not found at higher catalyst levels. Coprecipitated mixtures of metals show no advantage. Laboratory and commercial preparations of palladium are about equivalent. In short, palladium catalysts do not seem to have any advantage over platinum in high-performance electrode systems.

4. ELECTRODE DEVELOPMENT

4.1 High-Loading Electrodes

Data given in the First Quarterly Report[1] indicated that electrode performance might be improved by increasing the platinum loading, decreasing the waterproofing level, and utilizing single-screen structures. In order to explore these areas in greater detail, nine new electrode sheets with 40 mg/cm^2 loadings on single 40 mesh 10 mil wire nickel screens were prepared. Teflon level was 25% (standard) in three of the sheets, 14% in another three, and 8% in the remaining three sheets.

Each of these electrodes was evaluated against a counter-electrode of the same type, and for the 14% and 25% Teflon electrodes individually as hydrogen and as oxygen electrodes against standard Type AB-1 counter electrodes. Preliminary tests showed that with electrodes containing 8% Teflon, performance was erratic and poorer than with standard electrodes. Therefore, no further evaluation of the latter electrodes was made.

Averaged data for the electrodes containing 14% and 25% Teflon (same type on both sides of the cell) are presented in Table 4-1. Data for two standard AB-1 electrodes from recent production are included for comparison. A comparison among the averaged data for different sheets of the same type indicates a good degree of reproducibility in the electrode manufacturing process. The grand average data for all sheets of the same type indicate that 40 mg Pt/cm^2 electrodes containing either 14% or 25% Teflon give better than standard performance at low current densities. At high current densities, the 25% Teflon electrodes

TABLE 4-1

Performance of High-Loading Electrodes

1" Diameter Cell; 70°C; 5N KOH; Filter Paper Matrix; Test Electrodes Both Sides

Electrode No.	Pt. Loading mg/cm^2	Teflon Level %	No. of Tests	Ave. Cell Working Potential (Volts) at Indicated Current Density (ma/cm^2) 40	100	200	300	400
6609-5-1	40	25	3	.945	.908	.870	.847	.800
6609-9-1	40	25	4	.952	.913	.873	.842	.805
6609-9-2	40	25	3	.951	.913	.872	.839	.802
	Grand Average:		10	.950	.911	.872	.843	.802
	Standard Deviation:		10	.008	---	.007	---	.012
6609-8-1	40	14	3	.963	.921	.874	.832	.781
6609-9-3	40	14	4	.950	.906	.857	.817	.776
6609-9-4	40	14	3	.956	.914	.864	.819	.775
	Grand Average:		10	.955	.913	.864	.822	.777
	Standard Deviation:		10	.007	---	.017	---	.045
LD 213-365-16(1)	9	25	6	.930	.894	.855	.820	.781
6609-75-1(1)	9	25	3	.935	.897	.856	.819	.767
	Grand Average:		9	.931	.895	.855	.821	.777
	Standard Deviation:		9	.010	---	.008	---	.019

(1) Standard Type AB-1 Electrodes

give better results than those containing 14% Teflon. Actually, as shown by the standard deviations in Table 4-1, the electrodes containing 14% Teflon tend to perform more erratically.

To determine whether the improvement in performance noted for the high-loading electrodes was associated with the hydrogen or the oxygen electrode (or both), a series of tests was run in which high-loading electrodes were tested against standard counter-electrodes. The data are shown in Table 4-2. Because the difference in performance between standard and high-loading electrodes is small, it is difficult to draw firm conclusions. It does appear, however, that at low current densities, improvement in performance is associated with the oxygen electrode, and at high current densities, with the hydrogen electrode. At low current densities, the reaction mechanism at the oxygen electrode is probably performance-limiting. At high current densities, the ability of the hydrogen electrode to handle the correspondingly high rate of water production may well be critical. At any given time, a certain number of active catalyst sites in the hydrogen electrode are probably temporarily "deactivated" by adsorbed product water. At sufficiently high current densities, the number of available active sites may become limiting. Increasing the platinum loading at the hydrogen electrode may therefore improve performance at high current densities simply by making more active sites available for reaction.

4.2 Graded Waterproofing

Several electrodes having a graded waterproofing structure were prepared and evaluated. In these electrodes, the Teflon level was 35% on one face, and 8% on the other. It was thought that this type of structure might tend to stabilize the electrolyte-gas interface, and thus lead to improved performance in life tests. Initial polarization data for these

TABLE 4-2

Evaluation of High Loading Electrodes vs. Standard Counter Electrodes

1" Diameter Cell; 70°C, 5N KOH; Filter Paper Matrix

Oxygen Electrode:	40 mg Pt/cm² 25% Teflon		40 mg Pt/cm² 14% Teflon		Standard AB-1(1)		Standard AB-1(1)	
Hydrogen Electrode	Standard AB-1(1)		Standard AB-1(1)		40 mg Pt/cm² 25% Teflon		40 mg Pt/cm² 14% Teflon	
Total Data Points	4		4		5		3	
Current Density, ma/cm²	Cell Working Potential, Volts							
	Ave.	Std. Dev.	Ave.	Std. Dev.	Ave.	Std. Dev.	Ave.	Std. Dev.
40	.960	.002	.960	.006	.938	.001	.935	.001
100	.918	-	.922	-	.901	-	.898	-
200	.870	.003	.873	.020	.864	.002	.858	.004
300	.826	-	.832	-	.835	-	.826	-
400	.775	.009	.779	.050	.808	.004	.794	.012

(1) Electrode Sheet LD 213-365-16

electrodes, run with the low-waterproofing face toward the electrolyte, are shown in Table 4-3. Performance appears to be equivalent to that for electrodes having similar support structure and platinum loading, but with uniform waterproofing. Performance of these electrodes in life tests will be checked as time permits.

4.3 Expanded Nickel as Electrode Support

At the start of this report period, it was considered possible that the physical characteristics of expanded metal might contribute desirable properties to electrodes made with this material as support, resulting in increased cell performance, especially at higher platinum loadings. Expanded metal has a number of possible advantages over conventional woven screen. Since there are no individual wires, there are no contact points and the conductivity in the plane of the sheet should be improved. Also, the higher open area per unit weight allows higher catalyst loading or increased available active area per unit of geometric surface.

Expanded nickel sheets with from 25 to 625 openings/in^2 and thicknesses from 5 to 23 mils[(a)] were evaluated in this work. Small electrode sheets were prepared with both single and multiple thicknesses of expanded metal (sandwich structures) with total platinum loadings from 10 to 80 mg/cm^2 and Teflon levels of 10 to 40% based on platinum content.

Results of testing at ambient temperature are shown in Table 4-4 and are compared with a standard catalyst formulation at 9 mg Pt/cm^2 on conventional screen (listed at the top of the table). From the polarization data it will be seen that over the range of variables studied, there is no apparent advantage in using expanded metal instead of the standard woven screen.

(a) Obtained from Exmet Corporation, Bridgeport, Connecticut

TABLE 4-3

Evaluation of Electrodes with Dual Waterproofing Structure[1]

1" Diameter Cell; 70°C; 5N KOH; Filter Paper Matrix; Test Electrodes Both Sides

Electrode	S6609-1-2[2]	S6609-7-2	S6609-7-3	S6609-4-1[2]	S6609-8-2
Pt Loading, mg/cm^2	20	20	20	40	40
Teflon Level, %	25	8, 35	8, 35	25	8, 35
Support Screen	2 x 100 mesh "Sandwich"	2 x 70 mesh "Sandwich"	70 mesh Single Screen	2 x 70 mesh "Sandwich"	2 x 70 mesh "Sandwich"
Current Density, ma/cm^2	Working Voltage				
0	1.036	1.047	1.034	1.046	1.050
40	0.934	0.929	0.921	0.934	0.955
100	0.899	0.888	0.884	0.900	0.910
200	0.848	0.844	0.839	0.859	0.855
300	0.799	0.806	0.801	0.825	0.807
400	0.771	0.770	0.762	0.793	0.750

(1) Consisting of 8% and 35% Teflon on opposite sides, evaluated with 8% Teflon side toward electrolyte

(2) Data reported in first quarterly report

TABLE 4-4

Evaluation of Expanded Nickel as Electrode Support

As Oxygen Electrode vs. Standard Hydrogen Electrode

1" Diameter Cell; Ambient Temperature; 5N KOH; Filter Paper Matrix

Expanded Ni(1)			Total Platinum, mg/cm²	Teflon %	Cell Potential, Volts at		Run No.
Mesh, Openings/in²	Single Layer Thickness, mils	No. of Layers in Sandwich			40 ma/cm²	180 ma/cm²	S-6792
Standard AB-1 Expanded Nickel			9	25	0.925	0.835	
25	21	3	40	40	0.93	0.76	75-1
65	14	3	40	40	0.945	0.82	74-1
65	14	6	80	40	0.945	0.73	75-2
120	13	2	10	30	0.92	0.81	61-1
120	13	1	20	30	0.95	0.835	54-1
120	13	2	20	30	0.93	0.785	62-1
120	13	1	40	10	0.92	0.78	53-1
120	13	1	40	30	0.95	0.82	47-2
120	13	2	40	50	0.94	0.80	56-1
120	13	2	80	10	0.95	0.79	50-1
120	13	2	80	30	0.95	0.79	31-1
120	23	1	40	30	0.94	0.82	54-2
120	23	1	40	40	0.93	0.81	55-1
300	10	1	40	30	0.93	0.80	48-2
300	10	2	80	10	0.94	0.79	29-2
300	23	1	20	30	0.92	0.795	48-1
300	23	1	40	20	0.94	0.795	45-1
300	23	2	40	30	0.92	0.79	50-2
300	23	2	80	10	0.90	0.68	29-1
300	23	2	80	20	0.95	0.775	34-1
300	23	2	80	30	0.95	0.79	43-1
625	5	3	40	14	0.94	0.81	195-1
625	5	6	80	14	0.92	0.75	192-1

(1) Obtained from Exmet Corporation, Bridgeport, Connecticut

It can be concluded, however, that for expanded nickel 120 openings/in^2 gave better results than tighter mesh sizes (300 and 625 openings). More open mesh (65 and 25 openings) gave satisfactory catalyst retention only at a high Teflon level (40%) and even then performance was not as good as with 120 openings/in^2. The optimum range of waterproofing in this series appeared to be 20 to 30% Teflon.

5. TEST CELL DEVELOPMENT

5.1 Cell Design Modifications

To determine whether degradation of the silicone rubber gaskets or of the plastic film used to seal the edges of the matrix is a factor contributing to the voltage declines observed in the life-testing program, a 2" x 2" cell utilizing Teflon gaskets and matrix seal was designed. A comparison of the construction of this cell with that of the silicone rubber gasketed cell used in all prior work is shown in Figure 5-1.

The new cell design uses the same nickel face plates as were described in the First Quarterly Report[1]. When these plates are brought together, the Teflon gaskets join to form a gas and liquid-tight seal around the outer edge of the cell. The thin Teflon gasket deforms around the matrix to prevent gas leakage across the cell. The corrugated nickel screens are used to hold the electrodes against the membrane and also act as part of the current collector circuit. The use of corrugated screens eliminates the close thickness tolerance required for the spacer screens in the previous cell design. Since the Teflon gaskets come together at the edge, the need for a plastic film liquid seal is eliminated.

Life tests conducted in cells modified in the manner described above are discussed in Section 5.4.

5.2 Cell Assembly

Using a 2" x 2" cell of standard design (Teflon covered silicone rubber gaskets and polyethylene matrix seal), the effects of electrolyte loading and cell assembly pressure on cell resistance and performance were studied. Standard AB-1 electrodes and 20-mil Fuel Cell Asbestos were used. The tests were run at 70°C and atmospheric pressure, using 7N KOH.

CELL CONSTRUCTION

(Schematic – not to scale)

TYPE II (MODIFIED) CELL – TEFLON GASKETS

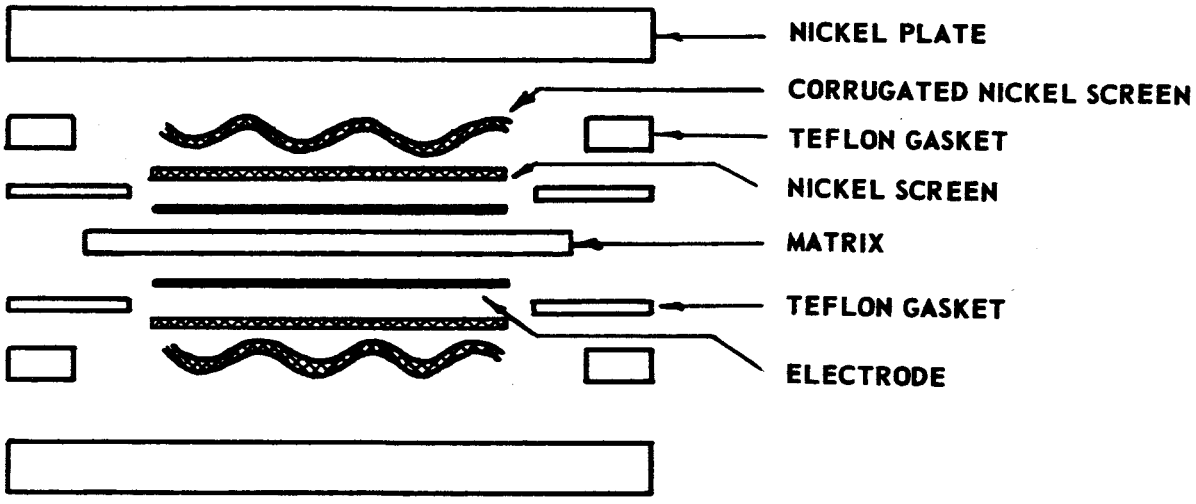

TYPE I (STANDARD) CELL – SILICONE RUBBER GASKETS

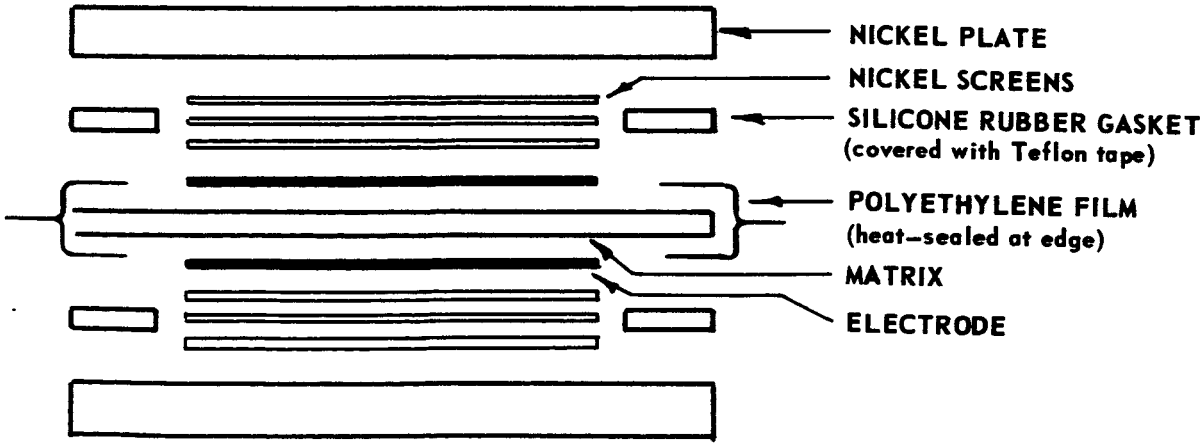

FIGURE 5–1

Table 5-1 shows the experimentally determined distribution of electrolyte between the matrix, the electrodes, and the spacer screens, for initial electrolyte loadings ranging from 0.25 to 1.5 grams KOH solution per gram dry asbestos. This distribution was essentially independent of cell assembly pressure in the range 60-180 psi. During assembly, 12-33% of the KOH solution initially loaded was pressed out of the matrix. Except at the highest intial loading, 80-90% of the rejected electrolyte was retained in the electrodes, while the remainder was retained in the spacer screens. The amount of electrolyte retained by the electrodes amounted to about 13-24% of the dry electrode weight, as compared to a "saturation" level of about 40%.

The effects of electrolyte loading and assembly pressure on cell internal resistance are shown in Figure 5-2. At an initial loading of 0.25 g/g, cell resistance is very high over the entire range of assembly pressure. Probably at this loading the electrolyte is not uniformly distributed over the entire matrix area. For this matrix material, the optimum conditions for minimum cell resistance appear to be at a loading of about 1.0 g/g and an assembly pressure in the range 120-180 psi.

Figure 5-3 shows the effects of electrolyte loading and assembly pressure on cell performance. As shown in the figure, performance at current densities above 100 ma/cm^2 falls off sharply as the electrolyte loading is decreased below 1.0 g/g. At a loading of 0.25 g/g, no current can be drawn from the cell. There is a general trend toward improved performance with increasing assembly pressure at all loadings above 0.25 g/g. At a loading of 0.75 g/g, a current density of 200 ma/cm^2 can be drawn only at the higher assembly pressures, 120-180 psig. The conditions for optimum cell performance

TABLE 5-1

Distribution of Electrolyte After Cell Assembly(1)

Initial Electrolyte Loading,	Amount of Electrolyte Retained in:					
	Matrix		Electrodes		Spacer Screens	
g/g(2)	g/g(2)	%(3)	g/g(2)	%(3)	g/g(2)	%(3)
0.25	.168	67	.066	26	.016	6
0.50	.398	80	.081	16	.021	4
0.75	.638	85	.098	13	.014	2
1.00	.880	88	.108	11	.012	1
1.50	1.25	83	.117	8	.133(4)	9

(1) Standard AB-1 electrodes, 20 mil Fuel Cell Asbestos. Assembly Pressure 60-180 psi.

(2) Grams solution/gram dry matrix

(3) % of electrolyte initially loaded.

(4) Some of electrolyte lost around edges of cell, since no matrix seal used in this case.

CELL INTERNAL RESISTANCE VS. ELECTROLYTE LOADING AND ASSEMBLY PRESSURE

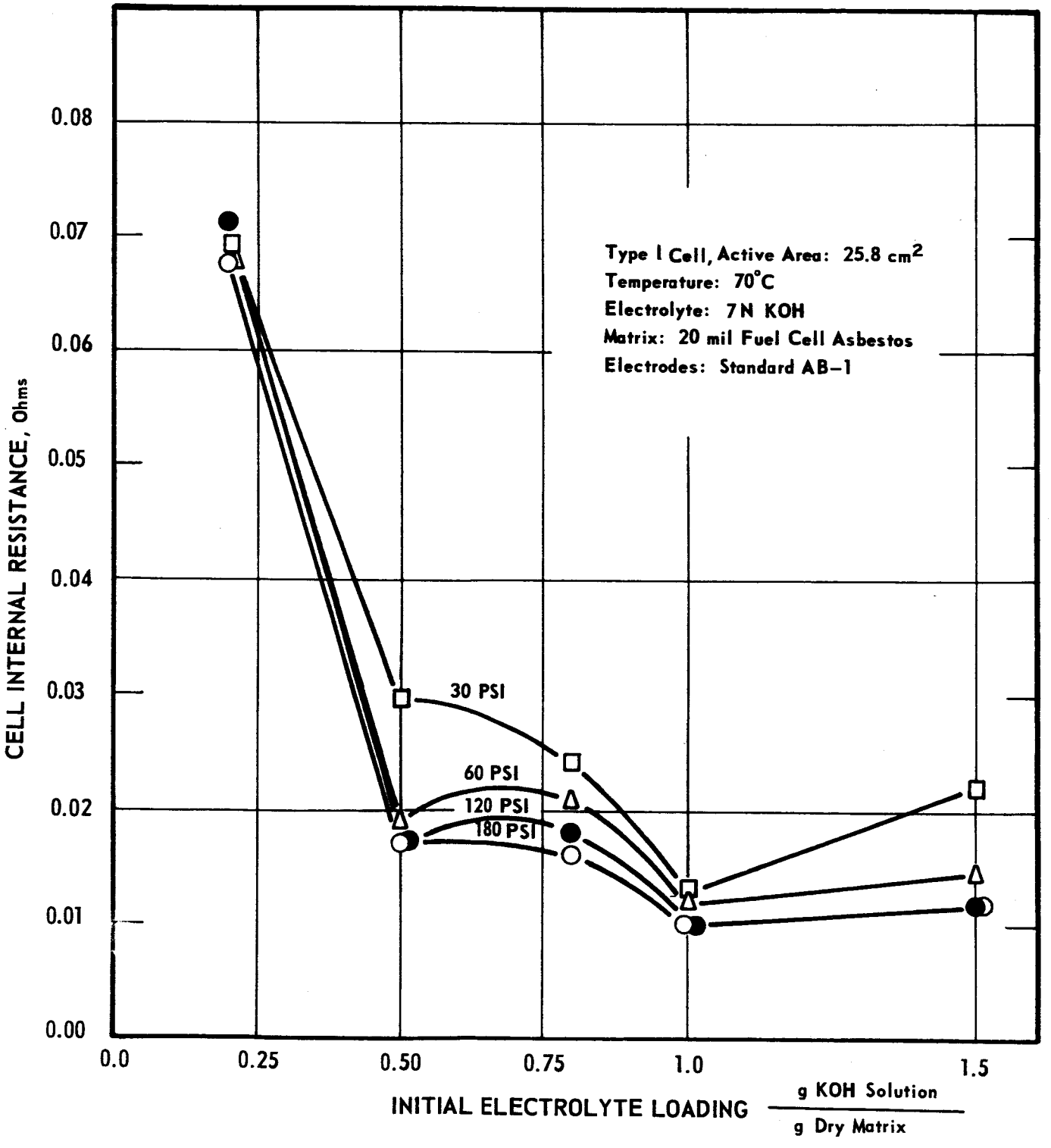

FIGURE 5-2

CELL PERFORMANCE VS. ELECTROLYTE LOADING AND ASSEMBLY PRESSURE

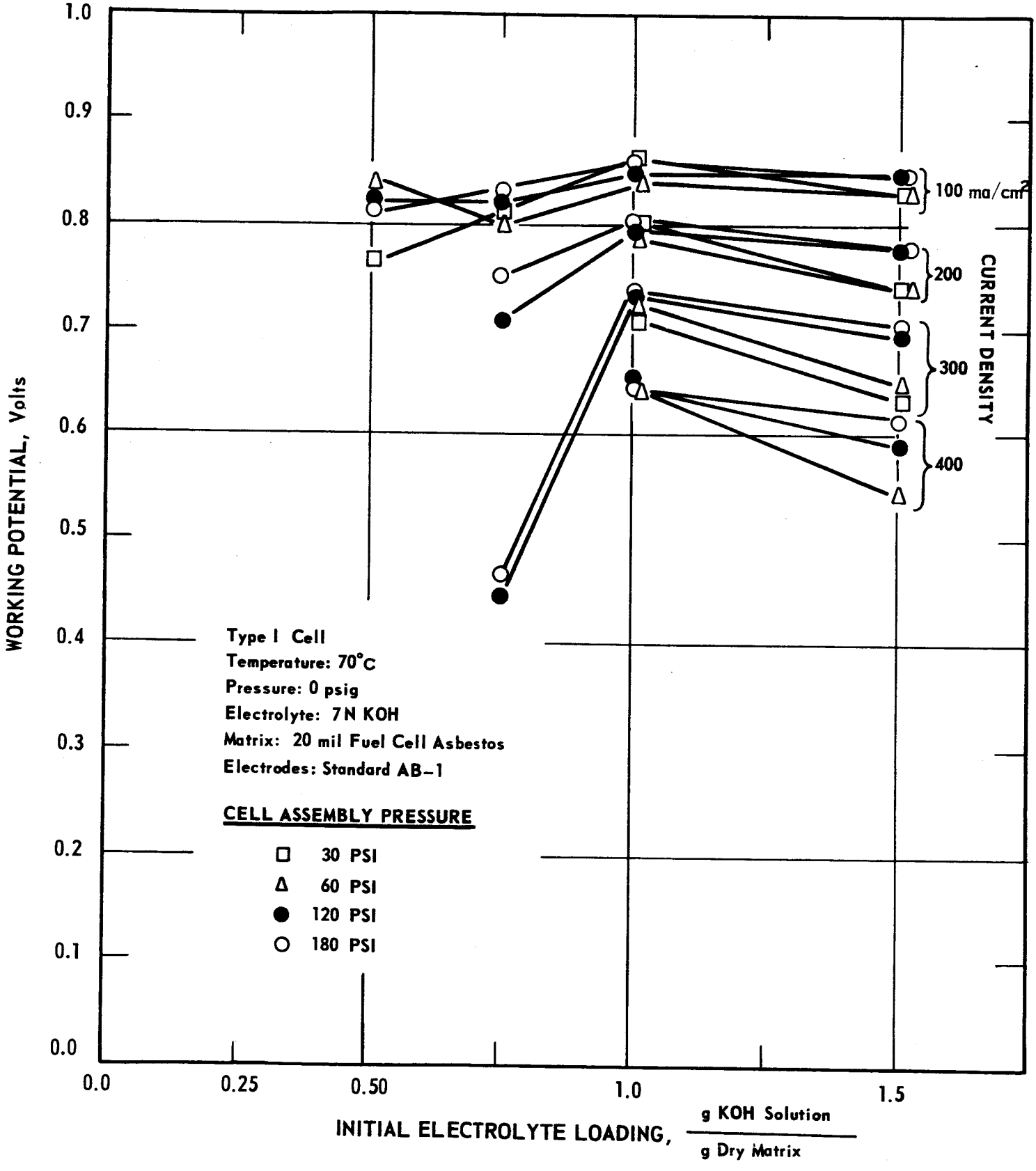

FIGURE 5-3

appear to be the same as already noted for minimum cell resistance, i.e., about 1.0 gram electrolyte solution per gram dry matrix and an assembly pressure of 120-180 psi.

5.3 Investigation of Operating Variables

The effect on fuel cell performance of a number of operating variables is being studied. This work is being directed toward determining a set of conditions which will maximize cell voltage and permit stable operation at high current densities. The principle variables under consideration are temperature, pressure, and electrolyte concentration. In addition, some very preliminary studies have been made on the effect of carbonate concentration in the electrolyte. To date, experimental work has been limited to 70°C, but extension of the present program to higher temperatures is planned.

5.3.1 KOH Concentration

The effect of KOH concentration over the range 1-13N was studied, using both standard AB-1 electrodes and high-loading (40 mg/cm^2, 25% Teflon) electrodes, together with 20-mil Fuel Cell Asbestos, or "ACCO" asbestos. The latter, as described in the First Quarterly Report, is more open than the Fuel Cell Asbestos and in equivalent thickness, gives a lower cell resistance.

For the Fuel Cell Asbestos, the optimum electrolyte loading described in Section 5.2 was used. With the less dense "ACCO" Asbestos, an initial loading of 2.0 gram solution per gram dry asbestos was employed. This is close to the "saturation" loading, and represents the same total weight of KOH as was used with the Fuel Cell Asbestos matrix. Cell assembly pressures of 120-180 psi were used with either matrix. Tests were run at 70°C in 1" cells.

In obtaining polarization data, the initial KOH concentration was maintained throughout the run by adjusting gas flows at each current density to maintain the water balance. Voltages were considered stable if they did not drop more than 3 millivolts during a two minute interval between readings.

For the four combinations of electrodes and matrix, the dependence of voltage on KOH concentration over a range of current densities is shown in Figures 5-4 through 5-7. At current densities below 100 ma/cm^2, voltage was in all cases relatively insensitive to concentration in the range 3-13N, although performance was generally slightly better at high normalities than at low. At current densities above 200 ma/cm^2, voltages became increasingly sensitive to KOH concentration, particularly with standard electrodes. With standard electrodes and 20-mil Fuel Cell Asbestos, stable performance at 400 ma/cm^2 was achieved only in a narrow concentration range centering around 5N. At 600 ma/cm^2, stable operation could not be obtained at any concentration (see Figure 5-4). With high-loading electrodes and "ACCO" asbestos, voltage was less sensitive to KOH concentration, and stable performance could be achieved at least out to 800-1000 ma/cm^2. With this system, performance as high as 0.8 volts at 400 ma/cm^2 was demonstrated (see Figure 5-7). It should be noted that the above discussion refers to short term stability only. Long term stability at high current densities remains to be demonstrated by life test.

The better performance obtained with the "ACCO" asbestos matrix was due in part to lower internal resistance. Figure 5-8 shows the relationship between cell resistance and electrolyte concentration for the four electrode-matrix combinations studied. Cell resistance did not vary with the type of electrode, and was little affected by electrolyte concentration in the range 3-13N.

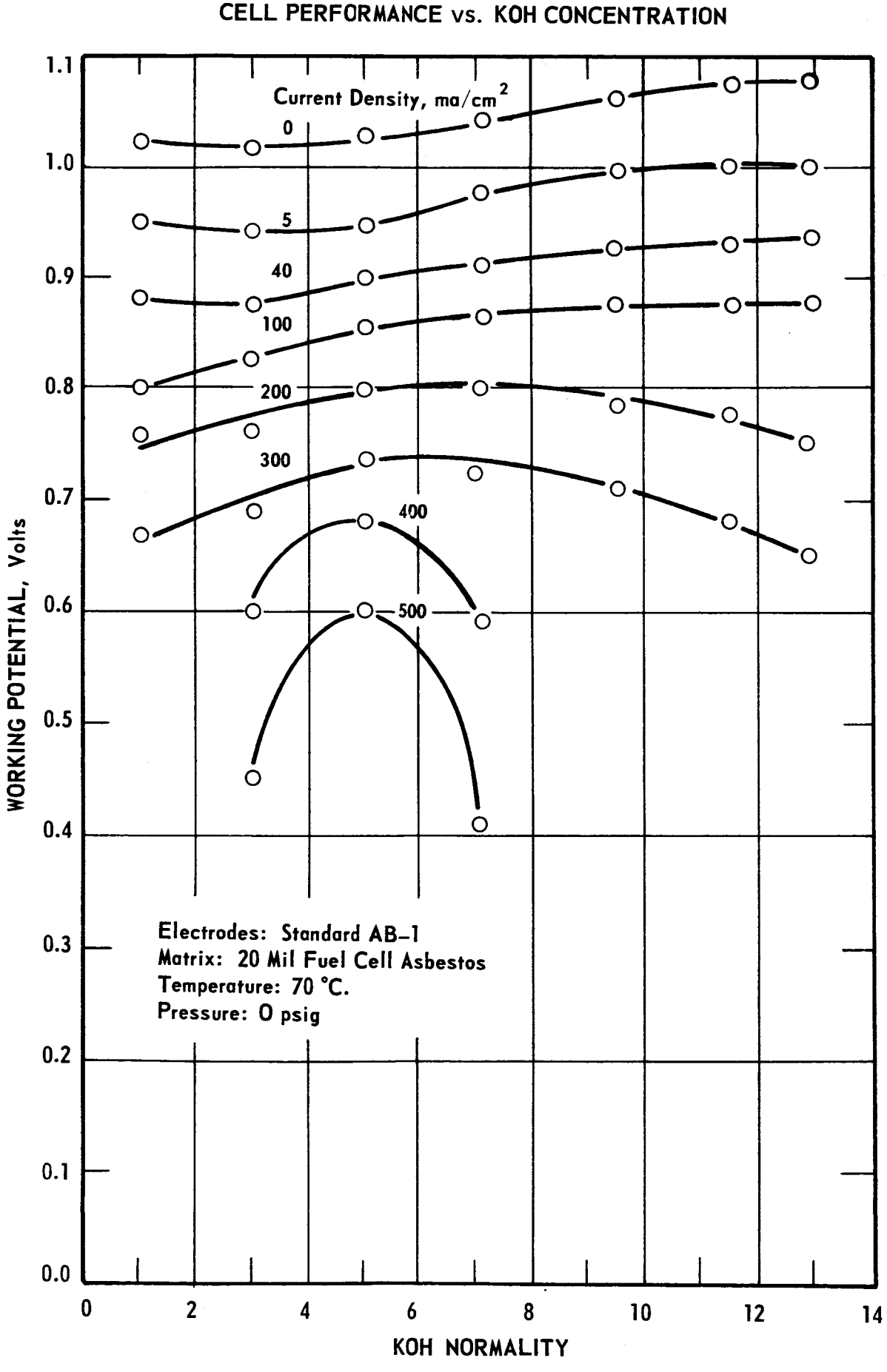
CELL PERFORMANCE vs. KOH CONCENTRATION
Current Density, ma/cm²
0
5
40
100
200
300
400
500
Electrodes: Standard AB-1
Matrix: 20 Mil Fuel Cell Asbestos
Temperature: 70 °C.
Pressure: 0 psig
WORKING POTENTIAL, Volts
1.1
1.0
0.9
0.8
0.7
0.6
0.5
0.4
0.3
0.2
0.1
0.0
0
2
4
6
8
10
12
14
KOH NORMALITY

FIGURE 5-4

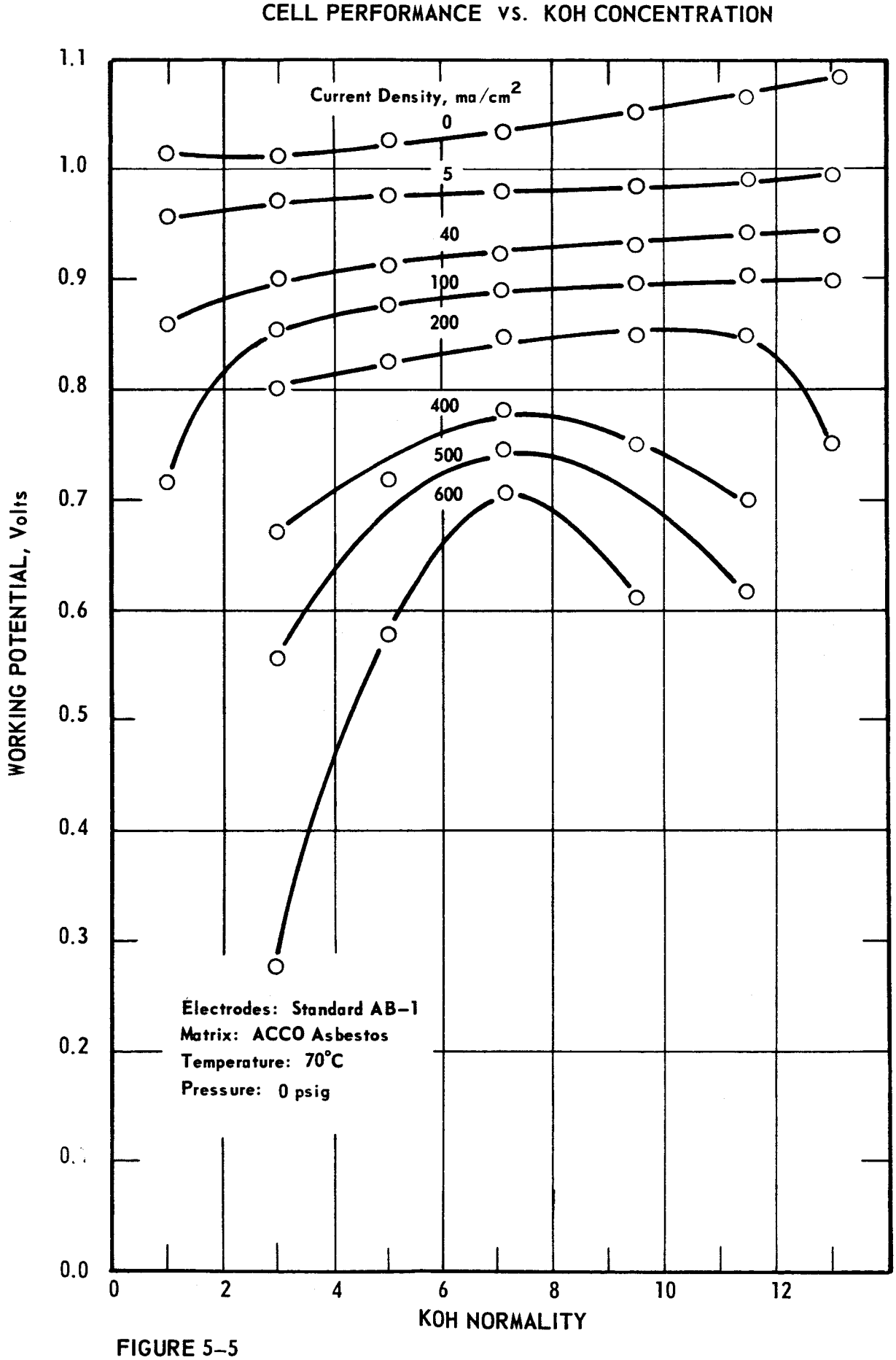
CELL PERFORMANCE VS. KOH CONCENTRATION
Current Density, ma/cm2
0
5
40
100
200
400
500
600
Electrodes: Standard AB-1
Matrix: ACCO Asbestos
Temperature: 70°C
Pressure: 0 psig
WORKING POTENTIAL, Volts
KOH NORMALITY
1.1
1.0
0.9
0.8
0.7
0.6
0.5
0.4
0.3
0.2
0.0
0
2
4
6
8
10
12

FIGURE 5-5

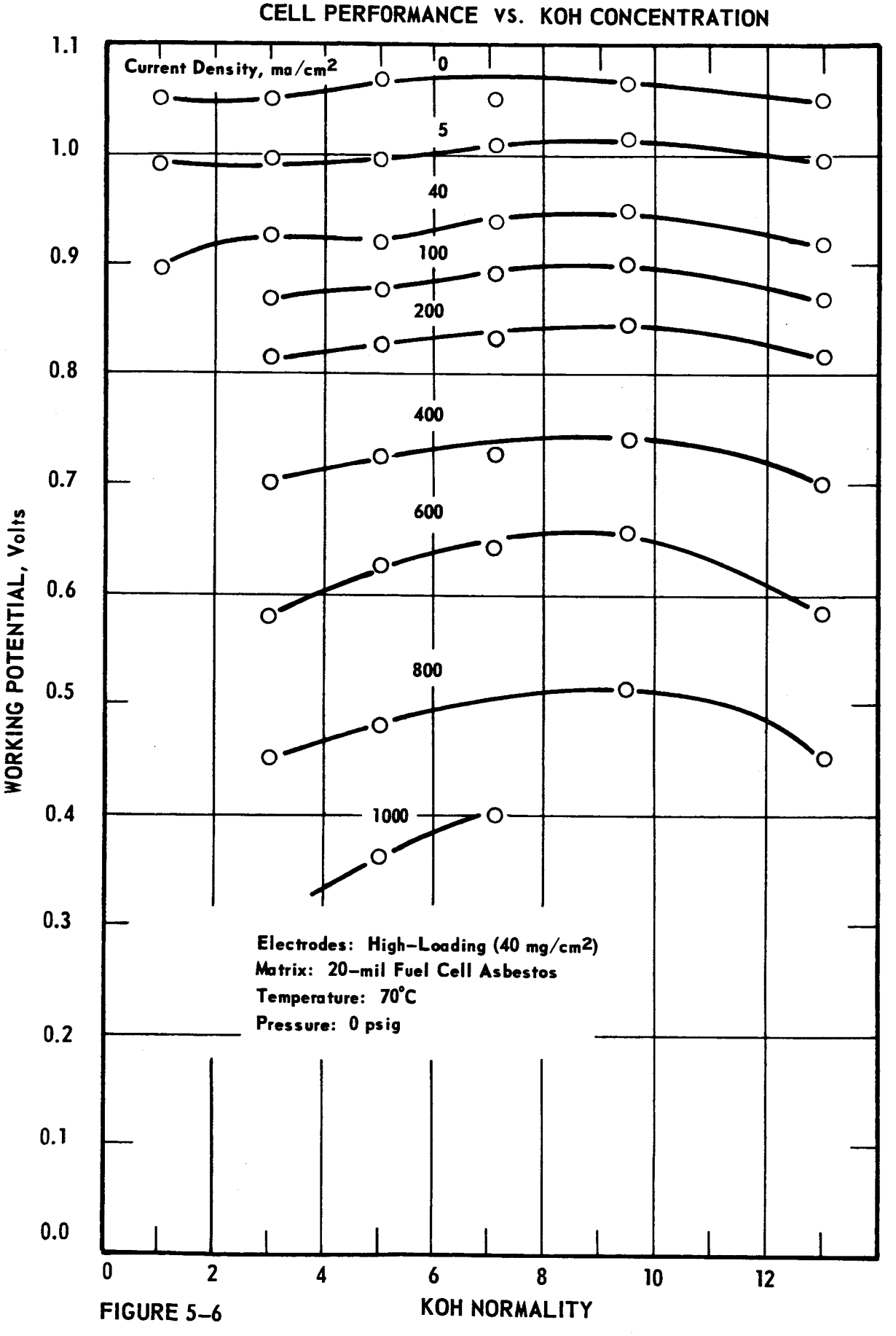
CELL PERFORMANCE VS. KOH CONCENTRATION
Current Density, ma/cm2
0
5
40
100
200
400
600
800
1000
Electrodes: High-Loading (40 mg/cm2)
Matrix: 20-mil Fuel Cell Asbestos
Temperature: 70°C
Pressure: 0 psig
WORKING POTENTIAL, Volts
1.1
1.0
0.9
0.8
0.7
0.6
0.5
0.4
0.3
0.2
0.1
0.0
0
2
4
6
8
10
12
KOH NORMALITY

FIGURE 5-6

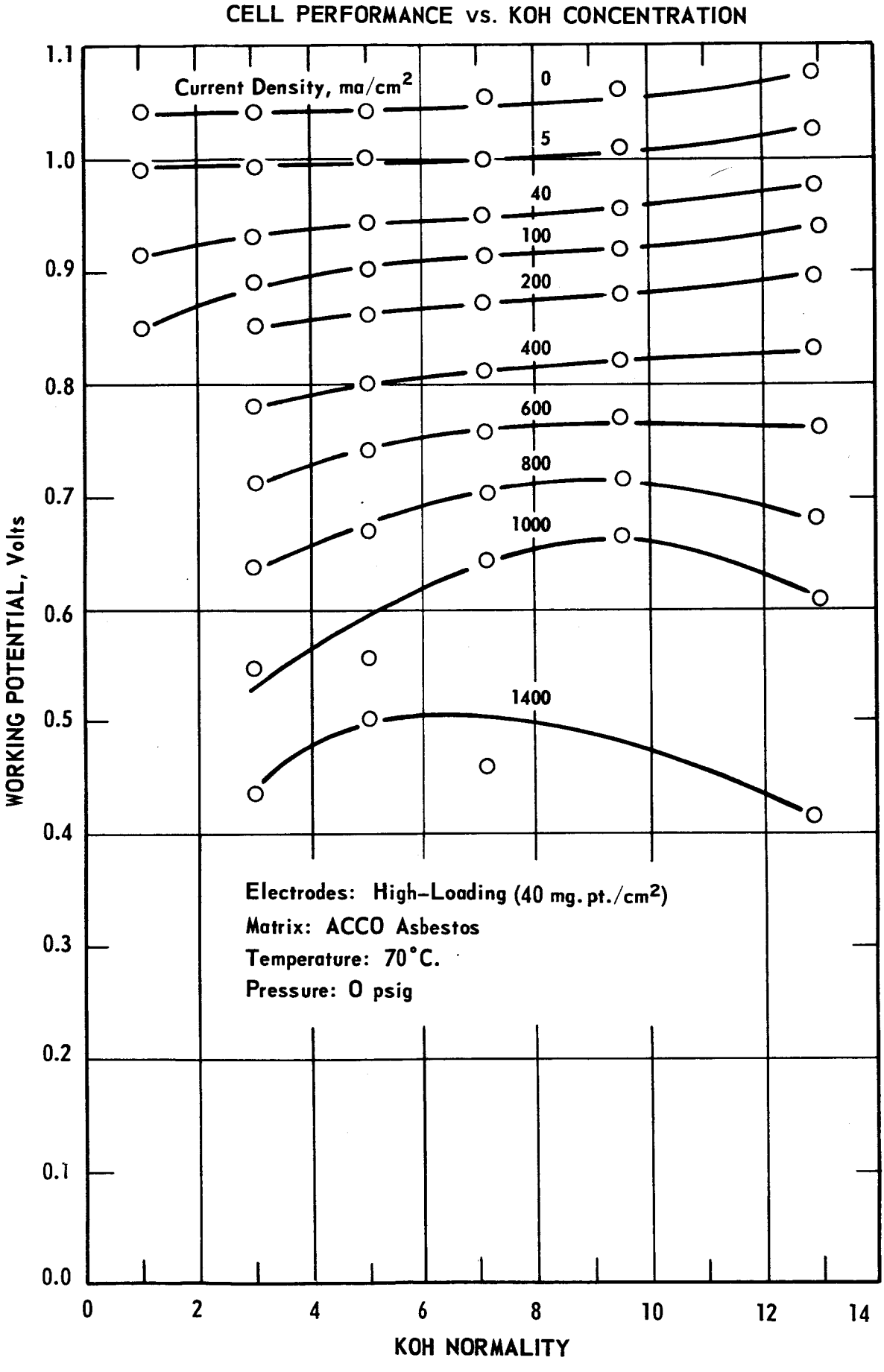
CELL PERFORMANCE vs. KOH CONCENTRATION
Current Density, ma/cm²
0
5
40
100
200
400
600
800
1000
1400
Electrodes: High-Loading (40 mg. pt./cm²)
Matrix: ACCO Asbestos
Temperature: 70°C.
Pressure: 0 psig
WORKING POTENTIAL, Volts
1.1
1.0
0.9
0.8
0.7
0.6
0.5
0.4
0.3
0.2
0.1
0.0
0
2
4
6
8
10
12
14
KOH NORMALITY

FIGURE 5-7

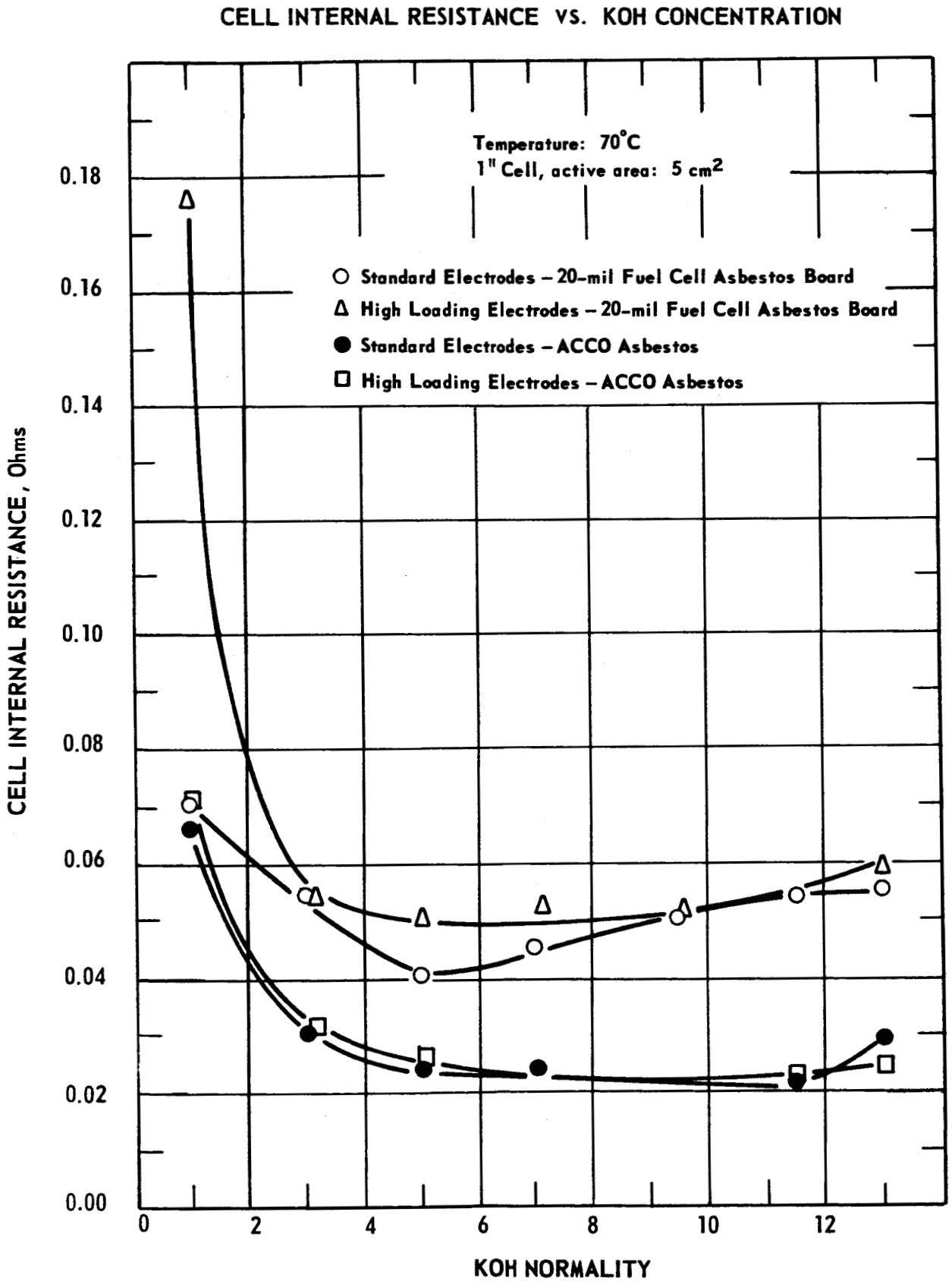
CELL INTERNAL RESISTANCE VS. KOH CONCENTRATION
Temperature: 70°C
1" Cell, active area: 5 cm²
Standard Electrodes – 20-mil Fuel Cell Asbestos Board
High Loading Electrodes – 20-mil Fuel Cell Asbestos Board
Standard Electrodes – ACCO Asbestos
High Loading Electrodes – ACCO Asbestos
CELL INTERNAL RESISTANCE, Ohms
0.18
0.16
0.14
0.12
0.10
0.08
0.06
0.04
0.02
0.00
0
2
4
6
8
10
12
KOH NORMALITY

FIGURE 5–8

However, the less dense ACCO matrix gave substantially lower cell resistance than the 20-mil Fuel Cell Asbestos. A thinner grade of Fuel Cell Asbestos would probably also give lower resistance and better initial performance, but there appear to be some difficulties associated with using thinner matrices in life tests (see Section 5.4).

5.3.2 Pressure

Some preliminary data has been obtained on the effect of pressure on cell performance at 70°C. Two tests were run, one with 30-mil and the other with 20-mil Fuel Cell Asbestos matrix. Standard electrodes were used in the former test, while in the latter, a high-loading oxygen electrode was used. The tests were run in 2" x 2" cells of the modified design described in Section 5.1, using C-clamps to prevent gas leakage. Polarization data were obtained at pressures up to 40 psig. Both tests showed that voltage increases with pressure, the increase being about the same over the whole current density range studied (0-200 ma/cm^2). At 100 ma/cm^2, a 35-40 millivolts increase was obtained by increasing the pressure from 0 to 20 psig, and an additional 15-20 millivolts by further increasing the pressure to 40 psig.

In order to extend the study of the effect of pressure to higher temperatures over a range of electrolyte concentrations, the cell described in Section 5.1 has been further modified to provide a wider gasket area and an increased number of bolts. Also, design of a cell suitable for life-testing under pressure has been started.

5.3.3 Carbonate Concentration

To determine the effect of carbonate on fuel cell performance, a series of polarization curves was run using as the electrolyte KOH solutions with varying K_2CO_3 content. Total solute concentration was kept constant at 34%. The K_2CO_3 concentration, expressed as a percentage of the total solute, varied from 0 to 100%.

The experimental data shown in Figure 5-9 indicate only a relatively small loss in performance with solutions containing K_2CO_3 up to about 44% of the total solute. (The solution is still approximately 3N in KOH.) At this level, cell voltage at 100 ma/cm^2 is about 30 millivolts lower than with "carbonate-free" KOH. When K_3CO_3 comprises more than 44% of the electrolyte, performance drops sharply, and is very poor for an electrolyte containing all K_2CO_3 and no KOH.

Based on the above data, it does not appear that the amount of carbonate normally present in reagent grade KOH (0.31-1.0%), or the amount which might be picked up by the electrolyte during cell assembly should present a problem. Of more concern, however, is the amount of CO_2 which might be brought in with the reactant gases, particularly in our life-testing program, where no recirculation of gases is employed. The CO_2 content of the oxygen used in life-testing is estimated to be about 6 ppm, based on studies of absorption in aqueous KOH. At the flow rates used, absorption by the electrolyte of all the CO_2 from the oxygen stream would convert as much as 20-25% of the KOH to carbonate in 1000 hours at 100 ma/cm^2. Actually, since Ascarite traps are used before the cell, and since contact between the bulk gas stream and the electrolyte is relatively poor, CO_2 pickup from the gas streams is probably much lower. Further tests are planned to determine how much carbonate actually accumulates in the matrix and how much is present in the exit gas stream.

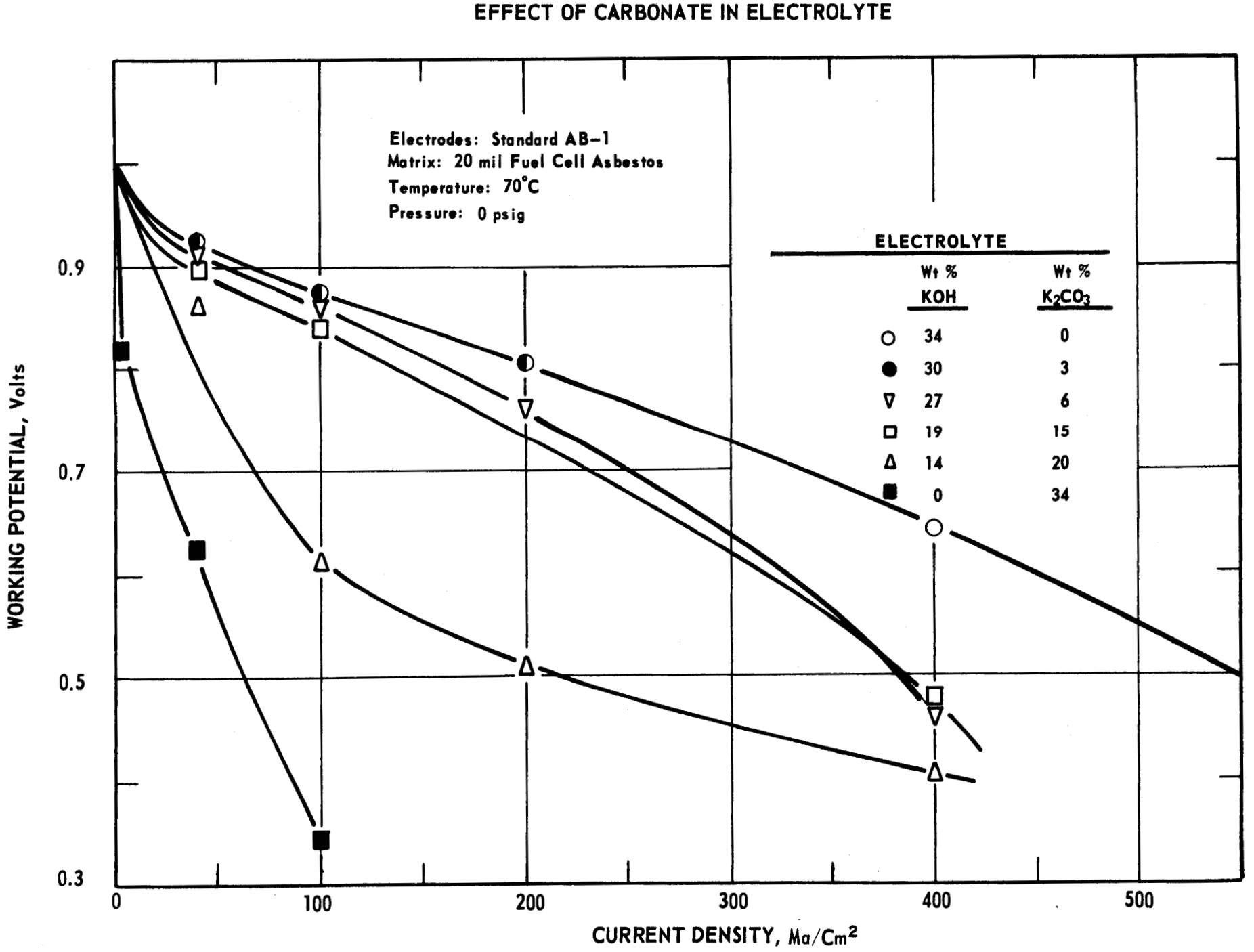
EFFECT OF CARBONATE IN ELECTROLYTE
Electrodes: Standard AB-1
Matrix: 20 mil Fuel Cell Asbestos
Temperature: 70°C
Pressure: 0 psig
ELECTROLYTE
Wt % KOH
Wt % K_2CO_3
34 0
30 3
27 6
19 15
14 20
0 34
WORKING POTENTIAL, Volts
0.9
0.7
0.5
0.3
0
100
200
300
400
500
CURRENT DENSITY, Ma/Cm²

FIGURE 5-9

5.4 Life-Testing

A summary of life tests run during the second quarterly period of this contract is given in Table 5-2. Using standard AB-1 electrodes, tests were conducted to evaluate the effects of changes in cell design, variations in type and thickness of the matrix, the use of presaturated inlet gases, and operation at a cell temperature of 100°C. Several additional tests were run to evaluate the performance of some experimental electrodes.

5.4.1 Tests with Standard Electrodes

Life test results reported in the First Quarterly Report indicated a slow decrease in voltage with time. Recent tests continue to show this trend. In most cases, too, an upward trend in cell resistance with time has been observed. The performance obtained over the first eight hundred hours of life test 6708-19, shown in Figure 5-10, illustrates these trends. During this period, an overall voltage decline of 65 millivolts or about 8 mv/100 hrs., occurred. During the same period, the cell resistance increased by about 11 milliohms to a value nearly double the initial cell resistance. Note, however, that at a total current of 2.6 amps (100 ma/cm^2), the IR drop corresponding to this increase in resistance accounts for only about 45% of the observed decrease in cell voltage.

5.4.1.1 Tests with Presaturated Gases

Three tests have been run at a cell temperature of 70°C with gases presaturated at 47°C. Under these conditions, the KOH concentration in the active area of the cell cannot exceed approximately 10.5N. In one test (6718-2), a standard cell configuration with Teflon-covered silicone-rubber gaskets and a polyethylene matrix-seal was used. Another test (6597-26) was run in a modified cell (see Section 5.1) having Teflon gaskets and matrix seals.

TABLE 5-2

LIFE TEST SUMMARY

2 x 2" Cells at 100 ma./cm.^{2}

Test No.	Cell Design[1]	Electrodes	Cell Temp.	Matrix	Initial Electrolyte Concentration	Inlet Gas Condition	Test Duration (hrs.)	Status	Cell Voltage Initial	Cell Voltage Now[3]	Remarks
6708-19	I	AB-1	70	FCAB 30[4]	7.2	Dry	1827	Continuing	0.845	0.813	Gases reversed after 808 hrs.
6718-2	I	AB-1	70	FCAB 30	7.2	Sat. at 47°C	1336	Terminated	0.847	0.695	
6708-33	I	AB-1	70	FCAB 10	7.2	Dry	1532	Terminated	0.687	0.812	Gases reversed after 1225 hrs.
6708-57	II	AB-1	70	FCAB 20	7.2	Dry	1198	Continuing	0.854	0.823	Gases reversed after 50 and 613 hrs.
6597-26	II	AB-1	70	FCAB 30	7.2	Sat. at 47°C	737	Continuing	0.800	0.817	
6597-42	II	AB-1	70	FCAB 30	5.0	H_2 sat. at 47°C O_2 "Dead-ended"	147	Continuing	0.822	0.789	All H_2O being removed on H_2 side
6708-47	I	AB-1	70	"ACCO" Asbestos	7.2	Dry	253	Terminated	0.822	0.791	Performance erratic
6708-76	II	AB-1	70	"ACCO" B-2[5]	5.0	Dry	217	Continuing	0.890	0.858	
6582-172	I	AB-1	100	FCAB 30	5.0	Dry	114	Terminated	0.864	0.62-0.75	Voltage and current oscillating
6582-178	I	AB-1	100	FCAB 30	5.0	Dry	115	Terminated	0.821	0.406	
6582-190	I	AB-1	100	FCAB 30	5.0	Dry	212	Terminated	0.815	0.736	
6582-120	I	AB-1	100	FCAB 30	8.0	Sat. at 79°C	303	Terminated	0.859	0.587	
6597-7	I	AB-40 mg./cm.^{2}	70	FCAB 10	7.2	Dry	1184	Terminated	0.854	0.482	
6682-104	I	H_2 : AB-1 O_2 : 50 mg. Ag./cm.^{2}	70	"ACCO" Asbestos	7.2	Dry	285	Terminated	0.854	0.482	
6718-16	I	H_2 : AB-1 O_2 : 40 mg. Ag./cm.^{2}	70	FCAB 30	7.2	Dry	1176	Terminated	0.78	0.70	
6582-162	Note[6]	H_2 : 55 mg. NiBlack/cm.^{2} O_2 : AB-1	100-115	FCAB 20	5.0	Dry	287	Terminated	0.86	0.28	Voltage above 0.8 for 250 hrs.

1. Cell design I uses Teflon-covered silicone rubber gaskets and polyethylene matrix seal. Design II uses Teflon gaskets and matrix seal (see Section 5.1)
2. 7.2 N KOH made from J. T. Baker KOH pellets containing 0.3% K_2CO_3 max. 5 and 8 N KOH solutions were purchased from Hartman-Leddon Co. and contain 300-400 ppm K_2CO_3
3. As of 9/1/64, or at termination
4. Johns Manville Fuel Cell Asbestos Board, in nominal 10, 20, or 30 mil. thickness
5. Proprietary membrane
6. Test run in 1" cell (5cm.^{2} active area)

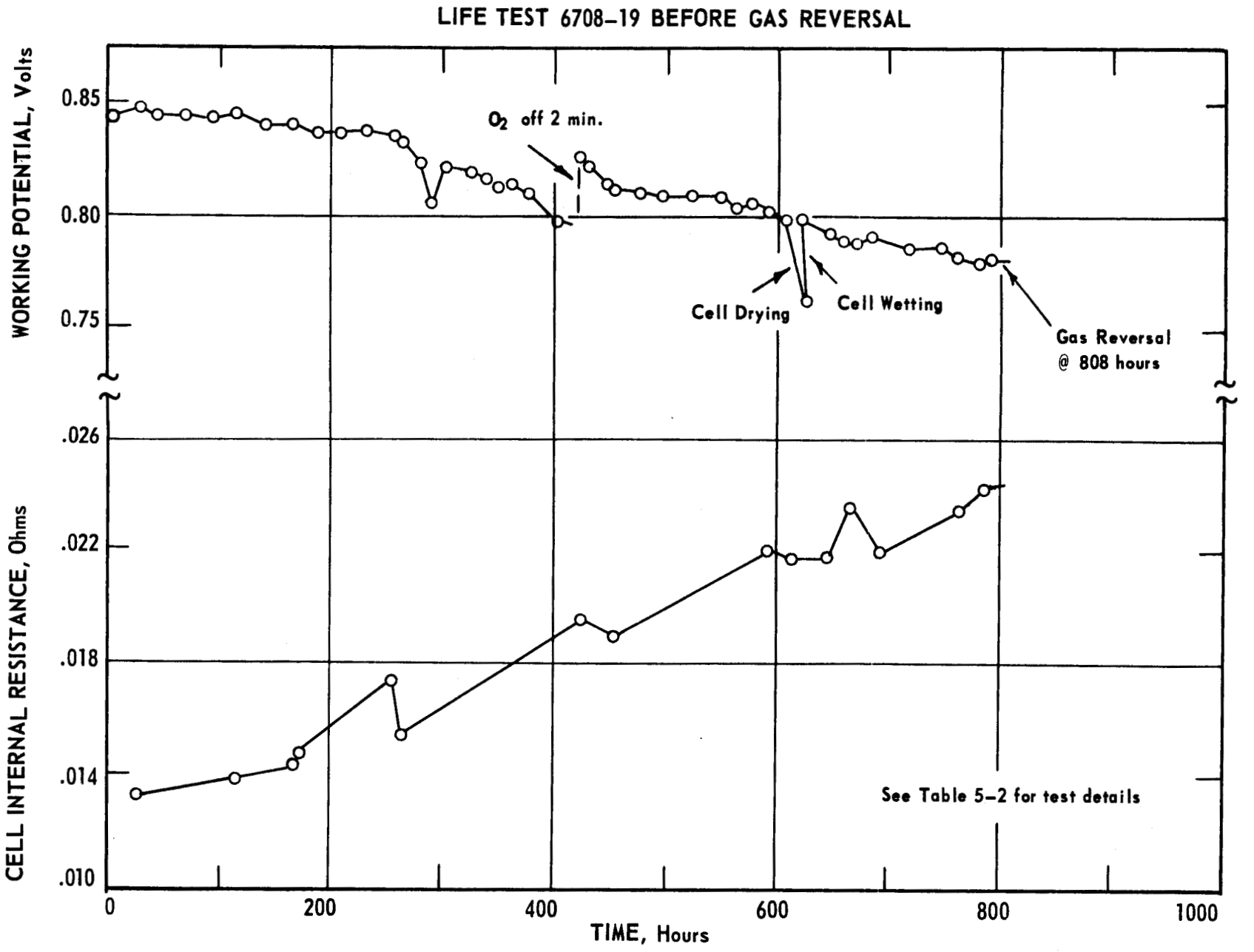
LIFE TEST 6708-19 BEFORE GAS REVERSAL
WORKING POTENTIAL, Volts
0.85
0.80
0.75
O_2 off 2 min.
Cell Drying
Cell Wetting
Gas Reversal
@ 808 hours
CELL INTERNAL RESISTANCE, Ohms
.026
.022
.018
.014
.010
See Table 5-2 for test details
0
200
400
600
800
1000
TIME, Hours

FIGURE 5-10

In both of these tests, downward trends in voltage and upward trends in cell resistance, similar to those observed in life test 6708-19, were encountered. Thus, it does not appear that these trends are associated with either (a) drying out around the inlet gas ports, as suspected on the basis of tests with dry gases, or (b) degradation of or contamination from silicone rubber or polyethylene cell parts.

In a third test (6597-42), gas flows were adjusted so that virtually all of the product water was removed by excess gas flow on the hydrogen side. Oxygen flow rate was set slightly above the stoichiometric requirement, thus providing a slow continuous purge without removing any appreciable amount of water. While this test has not been running long enough to provide a good comparison with other tests, the voltage drop during the first 147 hours appears to be unusually high.

5.4.1.2 Matrix Variations

In most of the tests run during this period, 30-mil thick Johns-Manville Fuel Cell Asbestos Board was used as the matrix. Because the IR drop observed with this thickness was appreciable, thinner sections of the same asbestos were also tested. In life test 6708-33, a 10-mil thickness was used. This test started at a higher level than did the tests with the thicker matrix, but showed the same general pattern of voltage decline. For a period of several hundred hours during this test, the water removed by the exit gases exceeded that formed electrochemically by about 20%, indicating leakage of gas through the matrix. In life test 6708-57, a 20-mil thickness proved more satisfactory. This test is discussed in more detail in Section 5.4.1.4.

In one test (6708-47) of the current series, "ACCO" asbestos was used. Performance was erratic, apparently as a result of gas leakage around the edges of the cell. Further life test evaluation of this asbestos is planned.

To determine whether the generally-observed loss in performance with time might be associated with a degradation of the asbestos matrix, one test (6708-76) has been started with an entirely different type of matrix. This matrix, a proprietary material designated by American Cyanamid Company as type B-2 Fuel Cell Membrane, consists of an ion-exchange resin embedded in an organic binder. With this matrix (approximately 25 mils thick), cell resistance and initial voltage were approximately the same as with the 10-mil Fuel Cell Asbestos. After 217 hours operation a downward trend in voltage and upward trend in cell resistance similar to those observed with asbestos matrices were evident. Thus it appears unlikely that the observed trends are caused by degradation of the matrix.

5.4.1.3 Tests at 100°C

Four tests were run at a cell temperature of 100°C, three with dry inlet gases and one with inlet gases presaturated at 79°C. In all of these tests, a more rapid decline in performance than in the 70°C tests was observed. This may be due partly to the greater difficulty in maintaining the water balance with dry gases at 100°C (the exit gas flow required to maintain an average concentration of 5N KOH at 100°C is only about 25% of the stoichiometric requirement). Deterioration of the polypropylene film used to seal the edges of the matrix also may have contributed

to the poorer performance at 100°C. In all tests, some degradation of the film was apparent upon disassembling the cell, and in life test 6582-178, deterioration of the film permitted water to escape around the edges of the matrix, resulting in over-drying the cell. The electrodes from life tests 6582-178 and 6382-172 were soaked overnight in water and re-evaluated. Those from 6582-178 had apparently lost some activity, while those from 6582-172 had not. Additional data are needed to determine whether there is a real loss of electrode activity at 100°C.

5.4.1.4 Effect of Gas Reversals

In several tests, interchanging the hydrogen and oxygen streams has been shown to have a beneficial effect on both voltage and cell resistance. Life test 6708-19, in which the hydrogen and oxygen were reversed after 808 hours, showed exceptional stability after the reversal. The first 800 hours of this test, illustrating the typical downward trend in voltage and upward trend in cell resistance with time, was shown in Figure 5-10. Figure 5-11 shows that after the reversal, voltage rose and stayed nearly constant at 0.825 $\pm$ .003 volts for approximately 600 hours. During this same period, cell resistance dropped to approximately the same value as at the start of the test, and then remained essentially constant. At 1580 hours total running time, the performance of this cell declined very rapidly. By reducing the gas flow rates, it was possible to stabilize the cell at a somewhat lower voltage. Since water balance is being maintained at the lower gas flow rates, it appears that there has been a loss of electrolyte from the active area of this cell.

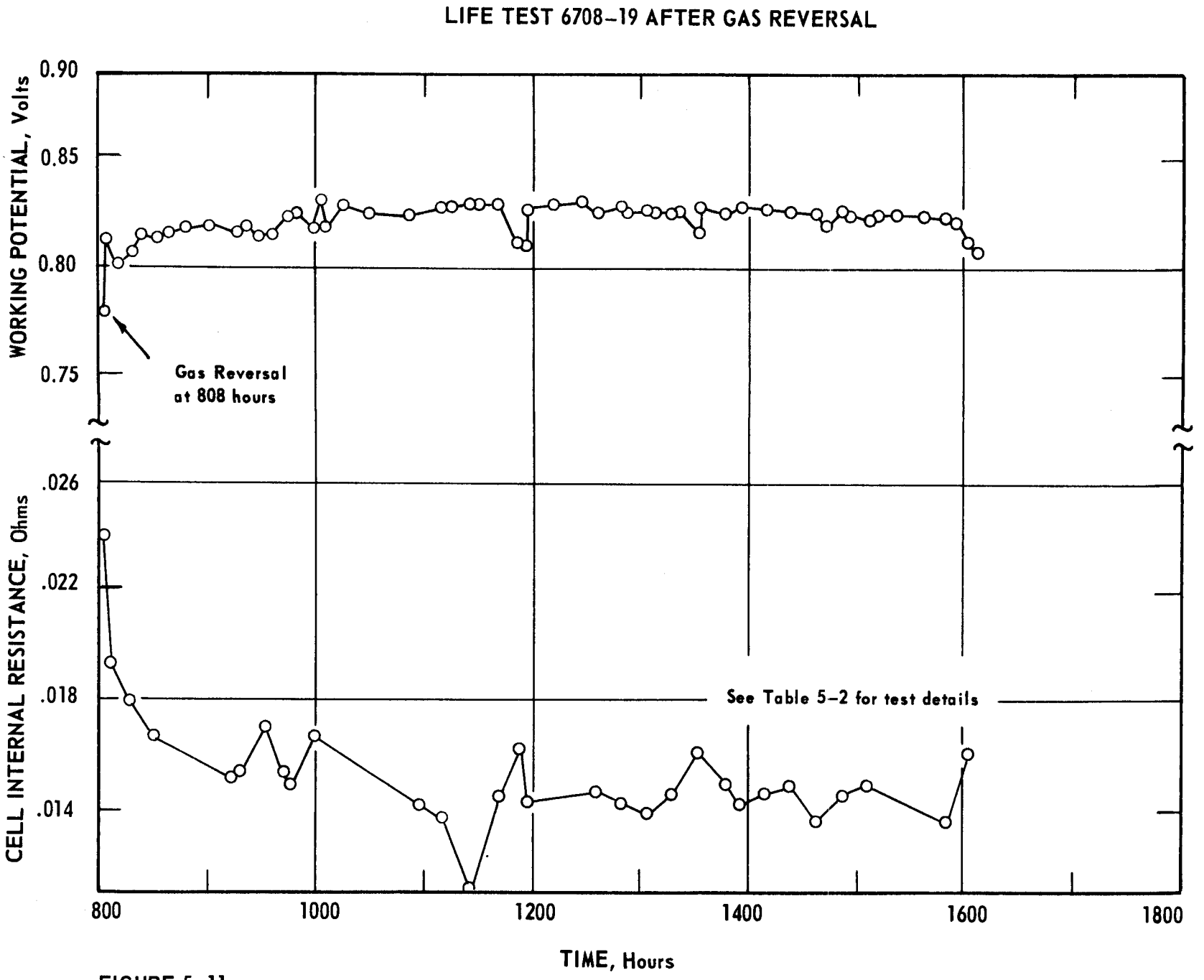
LIFE TEST 6708-19 AFTER GAS REVERSAL
WORKING POTENTIAL, Volts
0.90
0.85
0.80
0.75
Gas Reversal
at 808 hours
CELL INTERNAL RESISTANCE, Ohms
.026
.022
.018
.014
See Table 5-2 for test details
800
1000
1200
1400
1600
1800
TIME, Hours

FIGURE 5-11

Life test 6708-57 also showed more stable performance after reversing the hydrogen and oxygen streams. In this test, as shown in Figure 5-12, the gases were reversed twice; once after 50 hours, and again after 613 hours. After the first reversal, voltage and resistance remained stable for about 200 hours, after which the usual trends became evident. Following the second reversal, cell voltage has been stable at 0.824 ± .003 volts for approximately 600 hours, while cell resistance, which had been rising steadily, has dropped and remained essentially constant.

Similar effects were observed in life test 6708-33 on reversing the gases after 1230 hours, although in this case, the test was terminated shortly thereafter because of gas leakage through the matrix (10 mil Fuel Cell Asbestos).

The explanation for the observed more stable performance after gas reversal is not immediately evident. Since the cell itself is symmetrical (i.e. the same type of electrode on both sides) one would expect that, following a presumably short period of reorientation during which concentration gradients within the cell would be reversed, performance should then follow the same trends as before the reversal. This does not appear to be the case, however. It is hoped that further study of the effect of gas reversals may help explain the general performance trends noted in this life-testing program.

5.4.2 Tests with Experimental Electrodes

Life tests at 70°C, using dry gases, were run to evaluate (1) a high-loading platinum electrode and (2) silver oxygen electrodes. A life test was also run with a nickel black hydrogen electrode at 100-115°C.

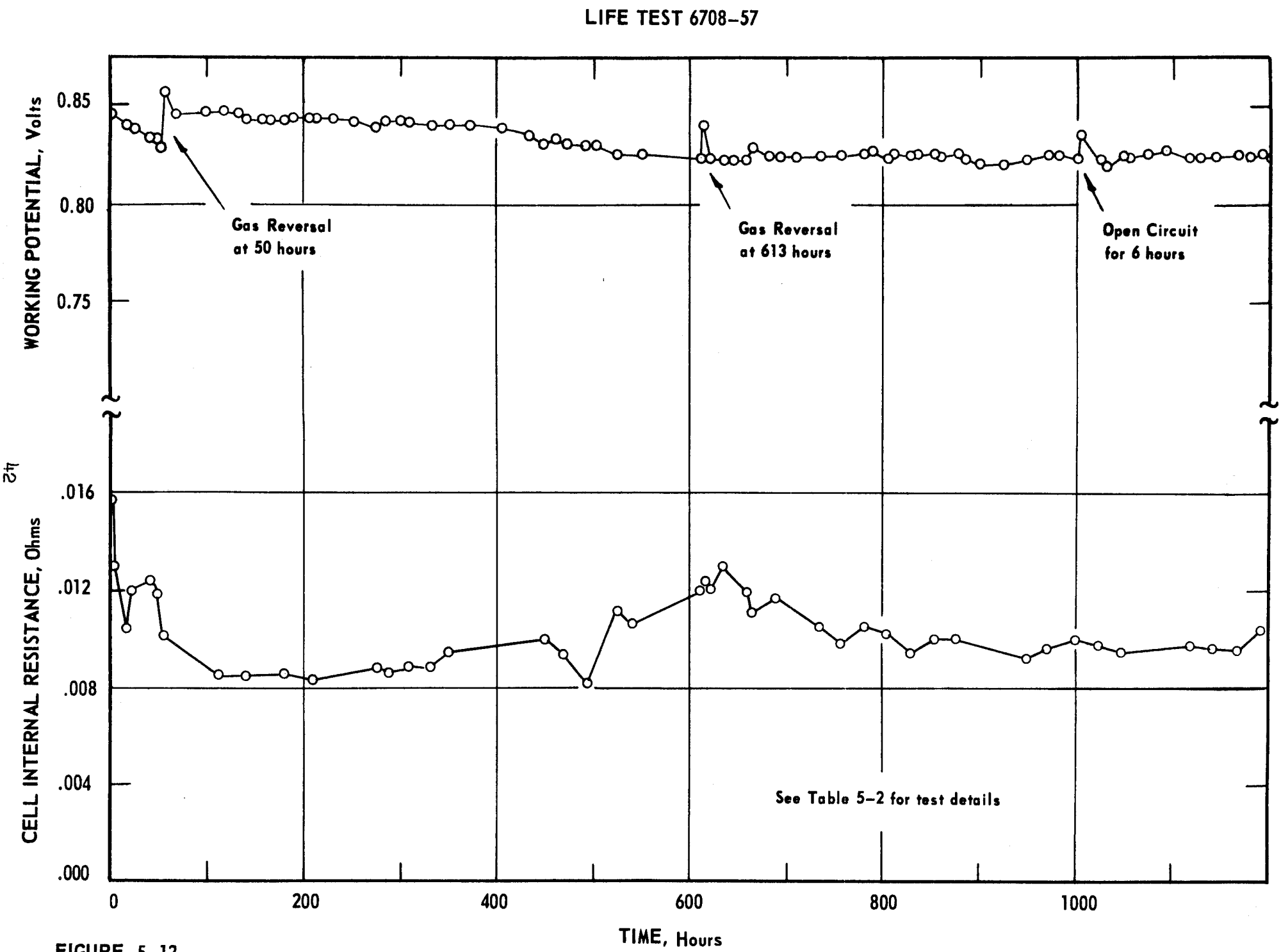
LIFE TEST 6708-57
WORKING POTENTIAL, Volts
0.85
0.80
0.75
Gas Reversal
at 50 hours
Gas Reversal
at 613 hours
Open Circuit
for 6 hours
CELL INTERNAL RESISTANCE, Ohms
.016
.012
.008
.004
.000
See Table 5-2 for test details
0
200
400
600
800
1000
TIME, Hours

FIGURE 5-12

The high-loading electrode (S-6609-5-1, containing 40 mg Pt/cm^2 and 25% Teflon) was one which had given superior initial performance (see Section 4.1 of this report). It was used at both hydrogen and oxygen sides in life test 6597-7. On life test, it gave a high initial performance, but showed a rate of decline similar to that for standard electrodes.

Two tests were run with silver electrodes. In both tests, a relatively rapid initial drop in performance was observed. In one test (6582-104), performance continued to decline and the test was terminated after 285 hours. Although performance had dropped to a low level, internal resistance had not increased appreciably. Evaluation of the electrodes after test indicated that the silver electrode had lost some activity, whereas the type AB-1 hydrogen electrode had not. In life test 6718-16, performance declined from about 0.78 volts to about 0.70 volts over the first 500 hours of test, and then remained at approximately that level for another 700 hours. Thus, silver electrodes can operate relatively stably over long periods of time, but their level of performance appears to be considerably below that attainable with platinum.

The test with a nickel black electrode (S-6449-41-1, approximately 55 mg/cm^2) was run in a one-inch diameter cell, using dry gases, at 100°C cell temperature (manually controlled). During the first 100 hours, despite temperature variations of $\pm$ 5°C, the voltage at 100 ma/cm^2 was maintained between 0.82 and 0.85 volts. The cell was then moved to a new location and the test continued, using a temperature controller. A voltage of 0.83-0.84 volts was maintained for approximately another 100 hours while gradually raising cell temperature to 115°C. Performance then dropped more rapidly, and the test was discontinued after a total of 287 hours. The nickel black electrode had changed in appearance to a greyish color. When reassembled in a fresh

cell it gave a much lower level of performance than originally, indicating that either the electrode itself is not stable at 100-115°C, or that it had become contaminated by degradation of other cell components at these temperatures. This question will be pursued further as a part of our program for life-testing at higher temperatures.

6. SCALE-UP

For single cell scale-up to a size (6" x 6" electrodes) in the range of battery dimensions, it is planned to simulate as closely as possible a cell operating within a battery stack. Cell design depends to a considerable degree upon the particular methods used for removing water and heat from the battery. Consideration therefore has been given to various possible systems.

In a dynamic system, water (and heat) are removed by a continuous flow of excess reactant gas, which is recycled to the system after condensing out water equivalent to that produced by electrochemical reaction in the cell. By proper selection of operating parameters, both heat and water balances can be satisfied by excess gas flows. In the more general case, however, some auxiliary cooling must be provided.

In a static system, water balance is maintained by evaporating water directly to space vacuum through a secondary membrane. This system involves no recirculation of excess gas. Auxiliary cooling is required to remove heat over and above that corresponding to the latent heat of evaporation of the product water. The auxiliary cooling (for either dynamic or static system) may be accomplished, for example, by fins around the periphery of the battery stack, or by circulating a coolant through the cell.

For space applications, the best methods for heat and water removal are those which require the simplest controls, and which minimize the weight-to-power ratio for the system. One of the principle objectives of this program is to provide electrodes for a system furnishing power at substantially less than 150 lbs/kw. Calculations have been made for

several methods of heat and water removal to determine whether a choice between methods can be made using system weight as a criterion.

6.1 Dynamic System of Water Removal

6.1.1 Dynamic System with Auxiliary Cooling

Battery parameters and ranges of operating variables considered are given below:

Gross power output:	2.4 kw
Net power output:	2.0 kw
Voltage	24 v
Current	100 amps
Current density:	100-500 amps/ft^2
KOH concentration:	3-13N
Pressure	1-3 atm
Cell temperature	50°-100°C

In the dynamic system, excess reactant gases, vaporizing water from the battery, are passed through a condenser-separator and recycled back to the battery. Make-up reactant gases are fed at a rate equal to their consumption by electrochemical reaction. Equipment requirements are less if only one reactant gas is recycled. For this study, it is assumed that hydrogen will be recycled, so that the water is removed on the same side of the cell as it is formed.

Figures 6-1 and 6-2 show, for two alternative means of auxiliary cooling, the principal components of a dynamic system. In Figure 6-1, cooling is accomplished by blowing air past fins on the battery, while in Figure 6-2, the primary coolant is circulated through the battery.

The weight and power consumption of the auxiliary components depend primarily upon (a) current density and (b) the difference in humidity between inlet and outlet gases. Increasing current density tends to decrease battery weight, but increases the weight and power consumption

DYNAMIC SYSTEM: AIR-COOLED BATTERY

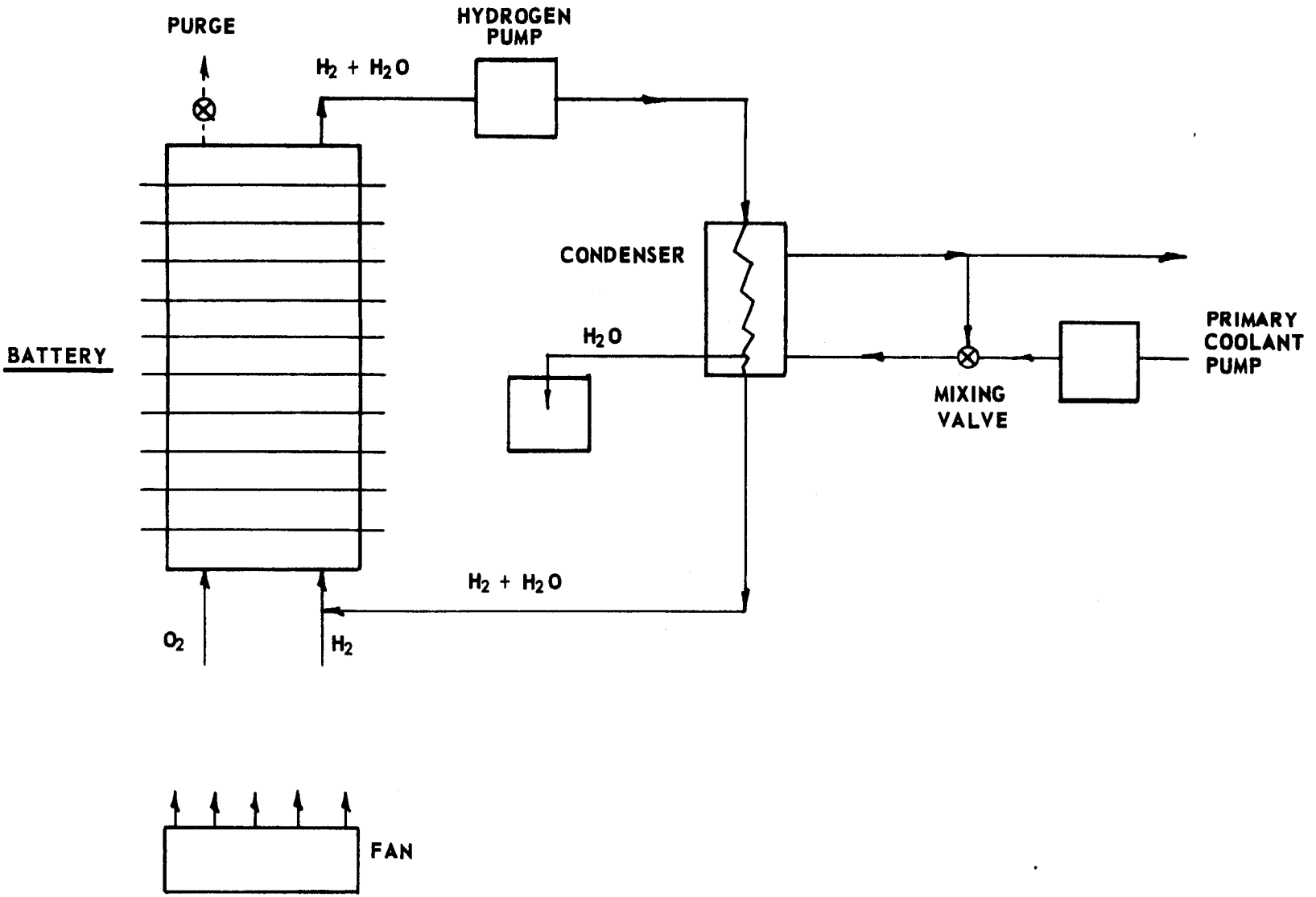

FIGURE 6-1

DYNAMIC SYSTEM: INTERNALLY COOLED BATTERY

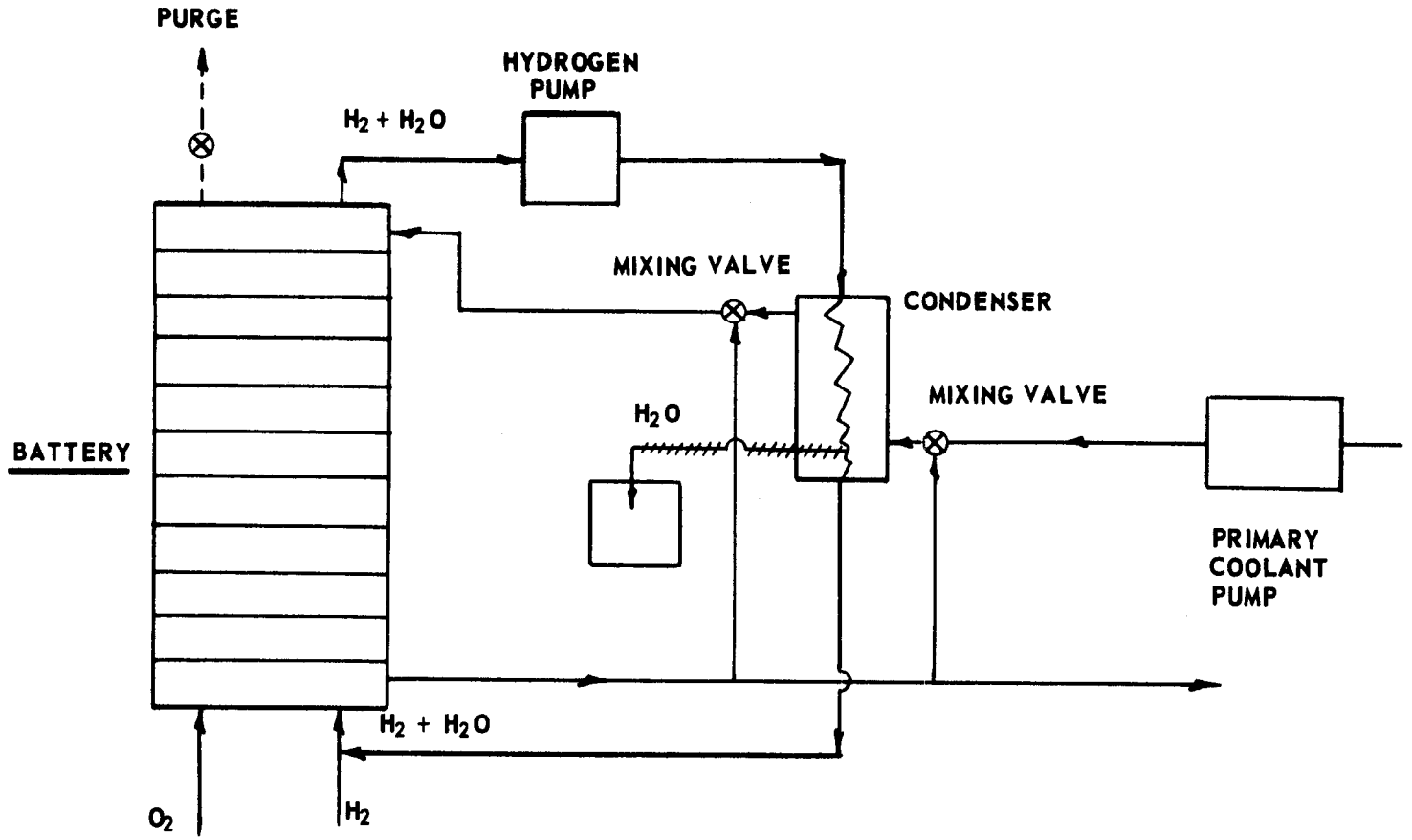

FIGURE 6–2

of the pumps or fans for recycle gas and battery coolant. Increasing the humidity difference tends to decrease the weight and power consumption of the gas recycle pump, but tends to increase the weight and power consumption of the coolant pump or fan. Any given humidity difference can be represented by many combinations of electrolyte concentration, battery and condenser temperature, and pressure, all of which have some separate influence upon the production and removal of waste heat. Nevertheless, the range of system weight per net power to be expected can be reasonably estimated by considering the four possible combinations of low and high current density and low and high exit gas humidity.

Table 6-1 shows the levels of current density and exit gas humidities considered, and the operating conditions chosen for each of the four combinations representing the two levels of these two parameters. For each battery temperature, a reasonable range of condenser exit temperatures was considered. Gases were assumed to leave the battery in equilibrium with the electrolyte concentration within the battery. Negligible pressure drop was assumed between condenser exit and battery inlet.

Table 6-2 shows the total heat generated by the battery and the distribution of heat effects. The total heat generated by the battery depends on the total current and the polarization at that current. Part of the heat is removed as latent heat of evaporation of water in the battery and as sensible heat required to heat both the incoming wet recycle hydrogen and the dry make-up gas; the remainder must be removed by auxiliary cooling. In terms of equipment, the heat load (over and above that removed as sensible heat by the make-up gases) is divided between the condenser and the auxiliary cooling means.

TABLE 6-1

Range of Operating Conditions

2 kw Dynamic System with Auxiliary Cooling

Condition	Current Density Amps/Ft²	Humidity $\frac{gH_2O}{gH_2}$ Battery Exit	Humidity $\frac{gH_2O}{gH_2}$ Battery Inlet	Temperature (°C) Battery (Average)	Temperature (°C) Condenser Exit	Pressure (Atm.)	KOH Normality	Volts/Cell
Low current density - Low battery humidity	100	0.32	0.14	50	32	3	3.0	0.87
	100	0.32	0.19	50	37	3	3.0	0.87
Low current density - High battery humidity	100	60.0	4.0	100	70	1	3.0	0.85
	100	60.0	7.7	100	80	1	3.0	0.85
	100	60.0	20.1	100	90	1	3.0	0.85
High current density - Low battery humidity	500	0.32	0.14	50	32	3	3.0	0.70
	500	0.32	0.19	50	37	3	3.0	0.70
High current density - High battery humidity	500	60.0	4.0	100	70	1	3.0	0.65
	500	60.0	7.7	100	80	1	3.0	0.65
	500	60.0	20.1	100	90	1	3.0	0.65

TABLE 6-2

Distribution of Heat Removal,
2 kw Dynamic System with Auxiliary Cooling

Condition	Condenser Exit Temp. (°C)	Total Heat Generated BTU/Min	% of Total Heat Removed by			
			Condenser		Sensible Heat of Make-up React.	Auxiliary Cooling
			Latent	Sensible		
Low current density - Low battery humidity	32	93.0	37	23	1	39
	37	93.0	37	23	1	39
Low current density - High battery humidity	70	98.0	34	0	3	63
	80	98.0	34	0	3	63
	90	98.0	34	0	3	63
High current density - Low battery humidity	32	148.0	29	17	1	53
	37	148.0	29	17	1	53
High current density - High battery humidity	70	171.0	26	0	2	72
	80	171.0	26	0	2	72
	90	171.0	26	0	2	72

Table 6-2 shows the distribution of heat loads to be independent of condenser exit temperature. Increasing condenser exit temperature increases the flow of wet recycle hydrogen required to maintain the water balance, but decreases the temperature differential between battery and condenser. As a result, the sensible heat removed by the recycle hydrogen is essentially constant. Since the sensible heat associated with the product water is small and the latent heat effect is constant, changes in condenser temperature over the range studied have no appreciable affect on the distribution of heat loads.

The probable ranges of pump and fan duties estimated for the four conditions considered are shown in Table 6-3. The estimates are based on an assumed ambient air temperature of 21°C, a primary coolant temperature of 21°C, and minimum temperature difference for heat exchange of 5°C (for example, a 5°C difference between gas inlet and coolant exit temperatures in the condenser). The ranges of flows shown in Table 6-3 for the hydrogen recycle pump and the condenser coolant pump correspond to the ranges in condenser exit temperatures considered.

Estimated weights and power consumptions for the major components of the battery system are given in Table 6-4. Table 6-5 shows calculated weight-to-power ratios for systems utilizing the various combinations of operating conditions and alternative cooling means previously discussed. The battery was assumed to be a stack of square

TABLE 6-3

Estimated Pump & Fan Capacities,

2 kw Dynamic System with Auxiliary Cooling

Condition	Current Density $\frac{\text{Amps}}{ft^2}$	Battery Humidity $\left(\frac{gH_2O}{g\ H_2}\right)$	Hydrogen Pump SCFM	Case I[1] Air Fan SCFM	Case I[1] Condenser Coolant Pump (G PM)	Case II[2] Battery & Condenser Coolant Pump (G PM)
Low Current Density-Low Battery Humidity	100	0.32	37-51	80	0.6 - 1.0	1.0
Low Current Density-High Battery Humidity	100	60.0	0.9 - 1.3	30	0.06-0.09	1.4
High Current Density-Low Battery Humidity	500	0.32	46-64	172	0.7 - 1.3	1.8
High Current Density-High Battery Humidity	500	60.0	1.2-1.7	59	0.08-0.11	2.8

(1) Auxiliary cooling by air flow past fins (Figure 6-1)

(2) Auxiliary cooling by internal flow of liquid coolant (Figure 6-2)

TABLE 6-4

Estimated Weight and Power Consumption of System Components,

2 kw Dynamic System with Auxiliary Cooling

Current Density[1]	Weight, (lb.)				Power Consumption, (Watts)			
	Low	Low	High	High	Low	Low	High	High
Battery Humidity[1]	Low	High	Low	High	Low	High	Low	High
Component								
Battery	70	70	34	34	-	-	-	-
Hydrogen Pump	90	20	90	20	108	9	133	12
Static Inverter, DC/AC	14	14	14	14	144	144	144	144
Condenser	2	1	2	1	-	-	-	-
Pressure Regulator	4	4	4	4	-	-	-	-
Solenoid Valve	1	1	1	1	-	-	-	-
Piping	5	5	5	5	-	-	-	-
Housing	11	11	11	11	-	-	-	-
Case I[2]: Air Fan	6	6	12	6	104	39	224	77
Coolant Pump	6	6	6	6	2	1	3	1
Mixing Valve	6	6	6	6	-	-	-	-
Case II[3]: Coolant Pump	6	6	6	6	3	4	5	7
Mixing Valve	12	12	12	12	-	-	-	-
Total, Case I	215	144	185	108	358	193	504	234
Total, Case II	215	144	191	108	255	157	282	163

Notes:

(1) See Table 6-1 for ranges of current density and humidity

(2) Auxiliary cooling by air flow past fins (Figure 6-1)

(3) Auxiliary cooling by internal flow of liquid coolant (Figure 6-2)

TABLE 6-5

Estimated Weight-to-Power Ratio,

2 kw Dynamic System with Auxiliary Cooling

Current Density[1] / Battery Humidity[1]	lbs/kw			
	Low Low	Low High	High Low	High High
Case I[2]	105	65	97	54
Case II[3]	100	64	90	48

(1) See Table 6-1 for ranges of current density and humidity

(2) Auxiliary cooling by air flow past fins (Figure 6-1)

(3) Auxiliary cooling by internal flow of liquid coolant (Figure 6-2)

cells, each 1/4" thick, with bipolar separator plates 2" longer and wider than the electrodes. The plates were assumed to be made of nickel-plated magnesium alloy. Pumps and fans were sized assuming a pressure drop of 5 inches of water for the air fan, 1 psi for the hydrogen recycle pump, and 3 psi for the liquid coolant pump. Pump and fan efficiency was assumed to be 50%. Approximate weights were obtained from manufacturer's data. The condenser was assumed to consist of a small stainless steel tube bundle in a plastic shell. The weight and power consumption of the static DC/AC inverter are based on estimates published by General Electric Co.[2] for inverters expected to be in operation within two years without technological breakthroughs.

As shown in Table 6-5, the estimated weight-to-power ratio for a dynamic battery system with auxiliary cooling is in the range 50-125 lbs/kw. The major sources of system weight and power consumption are the battery itself, the hydrogen recycle pump, and the static inverter. The air fan power consumption becomes significant at the condition of high current density and low exit gas humidity, partly because of the low battery temperature chosen to obtain low humidity. The weight and power consumption of the static inverter is independent of current density and humidity. Battery weight is estimated to decrease 50% by increasing the current density from 100 amps/ft^2 to 500 amps/ft^2 and to be independent of battery humidity.

There appears to be no significant difference, on a weight per unit power basis between air and liquid cooling. The greatest decrease in weight would come from reducing the recycle hydrogen pump capacity by operating at

high battery humidity. The hydrogen pump weights shown here are for steel pump construction. Special design and lightweight construction of the hydrogen pump would make the weight-to-power ratio less dependent upon battery humidity than shown in Table 6-4.

In order to achieve a weight-to-power ratio close to 50 lbs/kw, it will be necessary to operate at high battery humidity, i.e., with a battery temperature close to 100°C. For the same reason it will be desirable to operate with as low a KOH concentration as is consistent with good cell performance. Minimum electrolyte concentration will depend on the type of electrode and matrix used, as discussed in Section 5.3.

6.1.2 Dynamic System with No Auxiliary Cooling

An analysis has been made of a dynamic system in which both water and heat balances are maintained with excess reactant gas flow. The electrolyte matrix was assumed to support no gradients in either temperature or normality. Recycle gases (hydrogen or oxygen) were assumed to enter the cell saturated at some specified inlet temperature. Dry feed was assumed to enter at the same inlet temperature. The effluent gases were assumed to be in equilibrium with the electrolyte matrix. Under these conditions, the steady-state temperature and normality of the electrolyte can be computed explicitly after specifying four parameters:

1. absolute pressure, P, atm
2. inlet flow rate (dry basis) relative to stoichiometric requirements, F
3. inlet temperature, t_{in}, °C
4. current density, I, ma/cm^2

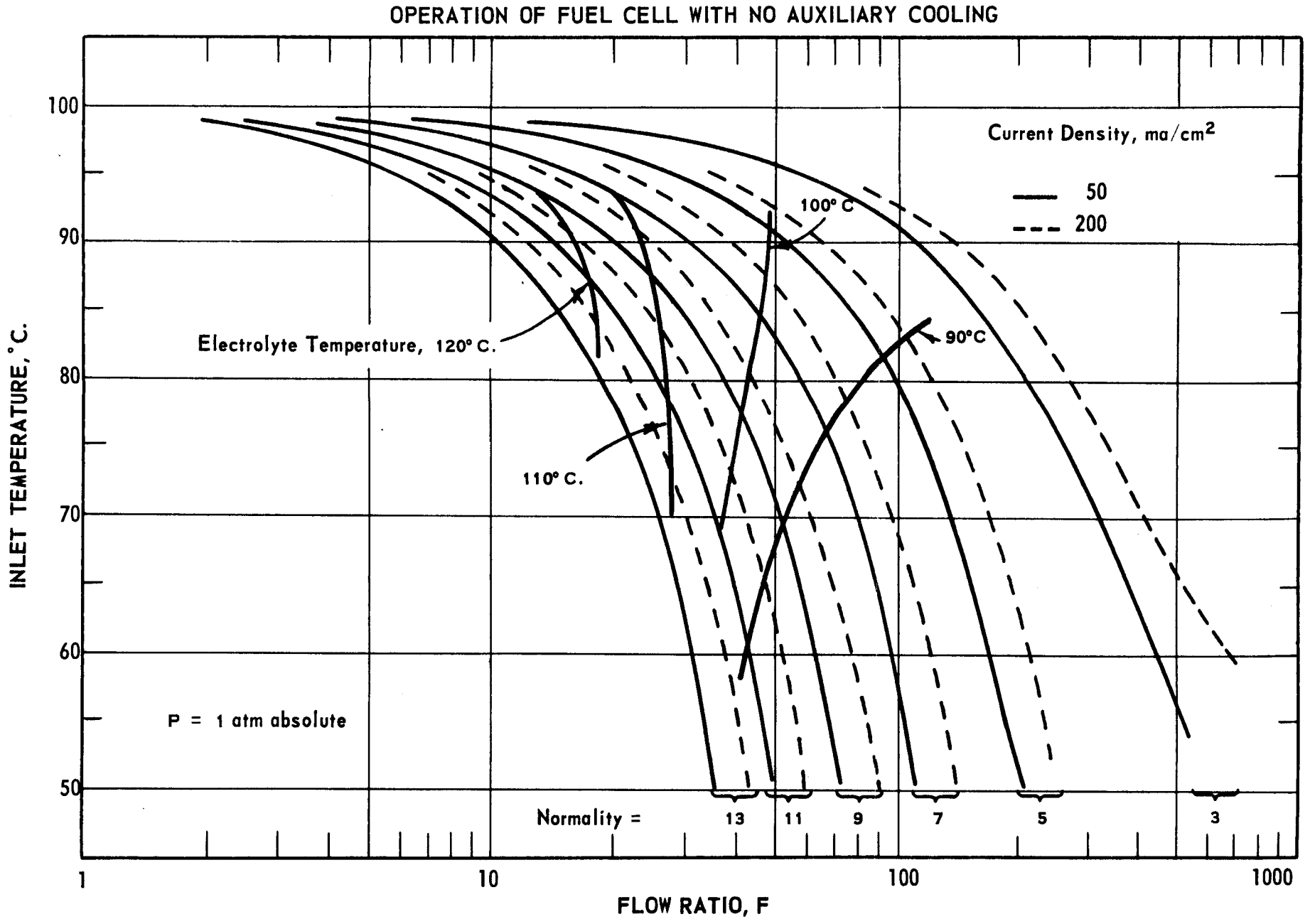
OPERATION OF FUEL CELL WITH NO AUXILIARY COOLING
INLET TEMPERATURE, °C.
100
90
80
70
60
50
1
10
100
1000
FLOW RATIO, F
Current Density, ma/cm²
50
200
100° C
90°C
Electrolyte Temperature, 120° C.
110° C.
P = 1 atm absolute
Normality =
13
11
9
7
5
3

FIGURE 6–3

The same F and t_{in} was used for both hydrogen and oxygen. The relevant equations were derived (Appendix), and together with the required correlations of physical properties were programmed for digital computation. Electrolyte temperature and normality were computed at P = 1 atm, F = 1 to 100, t_{in} = 50 to 99°C, I = 50 to 200 ma/cm^2. The basic results were then interpolated graphically to find combinations of inlet temperature and flow ratio that resulted in a constant normality. These contours covered the range over which a cell is likely to operate, 3 to 13N. The final results are plotted in Figure 6-3.

We see from Figure 6-3 that there is a broad range over which the cell can be operated within the limits of 3 to 13N. At a given inlet temperature and flow ratio, current density (between 50 and 200 ma/cm^2) has only a minor effect on cell normality. It must be emphasized, however, that flow rate is relative to stoichiometric requirements, and stoichiometric requirements are proportional to current density. Thus, we are assuming that in going for example, from 50 to 200 ma/cm^2, the absolute flow rate of the feed gases is increased 4 fold.

For space applications it is important to keep to a minimum the weight of the fuel cell package required to deliver a given amount of power to an external load. The fuel cell package consists of the cell, the fuel, and certain auxiliaries such as a water separator and gas recirculator. To reduce the direct weight of the water removal and gas circulation system, it is desirable to operate at the lowest practical flow ratio. Figure 6-3 shows that flow rates in the range 35-50 times stoichiometric are required to keep the battery temperature down to 100°C. By comparison, the calculations in section 6.1.1 show that at 100°C the flow rates required for water balance only are in the range 1 to 2 times stoichiometric.

A battery could be operated at flow ratios lower than 35-50 provided that electrolyte temperatures above 100°C could be tolerated. However, as the flow ratio is reduced below 10, electrolyte strength becomes very sensitive to inlet gas temperature. At a flow ratio of 5, for example, a variation of $\pm$ 2°C around the required inlet temperature of 98°C would be sufficient to permit the electrolyte concentration to vary over the whole range 3-13N.

From this study it appears that while a fuel cell battery could be operated with both heat and water balances maintained by excess reactant gas flows, the flow rates required would be very high. Since, as shown in Section 6.1.1, the gas recycle pump is a major weight factor in the battery system, this mode of operation may not be practical for space applications.

6.2 Static System of Water Removal

In the static water removal system, both hydrogen and oxygen can be dead-ended to each cell in the battery, and vented only occasionally to purge accumulated impurities. No gas recirculation equipment or condensers would therefore be required. If the water is rejected to space vacuum, the overall cooling requirements will be less for the static system than for the dynamic by an amount equal to the latent heat of vaporization. On the otherhand, auxiliary cooling (via fans or internal cooling) will be greater than for the dynamic system by an amount equal to the sensible heat removed from the recirculating gases in the condenser of the dynamic system. At 100°C battery temperature, the difference will be small, since the gas recirculation rate is low. At 50°C, however, the auxiliary cooling requirement for the static system would be 30-60% higher than for the dynamic system.

Because each cell of the static system requires additional components to accommodate the extra membrane, the battery itself of necessity will be heavier and occupy greater volume than for the dynamic system. If it is assumed that the battery weighs 50% more than the equivalent battery for the dynamic system, and that the weight and power requirements for auxiliary cooling are approximately proportional to the cooling load, then the weight-to-power ratio for a 2 kilowatt static system is estimated to vary from about 45 to 75 lbs/kw. With static removal, the current density at which the system operates is a major factor in determining battery weight, while battery humidity (or cell temperature) has only a small effect.

Based on this preliminary analysis, it appears that system weights of about 50 lbs/kw should be attainable with either dynamic or static water removal systems.

7. FUTURE WORK

Work planned for the third quarterly period will see continuation of Phase I of the Work Schedule, particularly the investigation of operating variables. Work will also be started on Phase II, involving scale-up to single cells of 6" x 6" size. The general plan is indicated below.

(a) Electrode Development

For the present, high-loading electrodes containing 40 mg Pt/cm^2 and 25% Teflon will be considered as the new standard electrode for use in the life-testing and scale-up programs. Further electrode development will be limited to that required for optimizing performance in the life-testing program.

(b) Effect of Operating Variables

Work in this area will be continued in order to define the inter-relationships between temperature, pressure, and electrolyte concentration. A preliminary investigation of the static water removal system on a 2" x 2" scale is planned.

(c) Life-Testing

Further work in the life-testing area will emphasize higher temperatures (to 100°C) and higher current densities (to 400 ma/cm^2). A vehicle for life-testing under pressure will be designed and fabricated. The long-term stability of "ACCO" asbestos will be studied.

(d) Scale-up

(1) A single cell for preliminary evaluation of electrodes on a 6" x 6" scale will be built and tested. Cell design will be generally similar to designs currently used in the life-testing program, and will be based on the dynamic water-removal concept.

(2) Analysis of heat and mass transfer problems will continue, with emphasis placed on determining the best gas distribution and heat removal configurations to minimize temperature and concentration gradients.

(3) A prototype bipolar separator plate, scaled for a 2 kilowatt battery, will be designed. The design will emphasize light-weight construction, and will be based on the analysis of heat and mass transfer problems described in the preceding paragraph.

APPENDIX

Performance Equations for Dynamic System with No Auxiliary Cooling

Hydrogen consumed, G mole/cm^2-hr =

$$\frac{3600 \text{ sec/hr}}{96494 \frac{\text{amp-sec}}{\text{G equiv}}} \times \frac{1}{2} \frac{\text{G mole}}{\text{G equiv}} \times \frac{1 \text{ amp}}{1000 \text{ ma}} \times \frac{I \text{ ma}}{cm^2}$$

$$= 1.865 \times 10^{-5} I$$

Hydrogen in = $F(1.865 \times 10^{-5} I)$

Hydrogen out = $(F-1)(1.865 \times 10^{-5} I)$

Oxygen consumed = $\frac{1}{2}(1.865 \times 10^{-5} I)$

Oxygen in = $\frac{F}{2}(1.865 \times 10^{-5} I)$

Oxygen out = $\frac{1}{2}(F-1)(1.865 \times 10^{-5} I)$

Water produced = $1.865 \times 10^{-5} I$

Water in via fresh gas = 0.

Water in via recycle gas = $\frac{p(0, t_{in})}{P-p(0, t_{in})} \frac{3}{2}(F-1)(1.865 \times 10^{-5} I)$

Water out = $\frac{p(N, t_{out})}{P-p(N, t_{out})} \frac{3}{2}(F-1)(1.865 \times 10^{-5} I)$

All of the above flows are in G mole/cm^2-hr

$p(N, t)$ = vapor pressure of water over KOH solution of normality N, at temperature t °C.

P = total pressure

Making a water balance and solving for $p(N, t_{out})$

$$p(N, t_{out}) = P \left[\frac{\frac{p(0, t_{in})}{P-p(0, t_{in})} + \frac{2/3}{F-1}}{1 + \frac{p(0, t_{in})}{P-p(0, t_{in})} + \frac{2/3}{F-1}} \right] \qquad (1)$$

which holds for all $I>0$; $F>1$; $P>p(0, t_{in})$

Enthalpy input, cal/cm^2-hr

$$6.96\,(t_{in} - 18)F(1.865 \times 10^{-5}\, I) + 7.13(t_{in} - 18)\frac{F}{2}(1.865 \times 10^{-5}\, I)$$

$$+\left[8.10\,(t_{in} - 18) - 57{,}801.\right] \frac{p(0, t_{in})}{P-p(0, t_{in})} \frac{3}{2} (F-1)(1.865 \times 10^{-5}\, I)$$

in which the first term is the enthalpy of incoming hydrogen, the second term is the enthalpy of incoming oxygen and the last erm is the enthalpy of incoming water.

Rearranging, enthalpy in =

$$\left\{10.53\,(t_{in} - 18)\,F + \left[12.15\,(t_{in} - 18) - 86{,}702.\right](F-1)\,\frac{p(0, t_{in})}{P-p(0, t_{in})}\right\}$$

$$\times\,(1.865 \times 10^{-5}\, I)$$

Similarly, enthalpy out with effluent gas =

$$\left\{10.53\,(t_{out} - 18) + \left[12.15\,(t_{out} - 18) - 86{,}702.\right]\frac{p(N, t_{out})}{P-p(N, t_{out})}\right\}$$

$$\times\,(F-1)(1.865 \times 10^{-5}\, I)$$

Enthalpy out as electrical power, cal/cm^2-hr =

$$860.4\ \frac{\text{cal}}{\text{volt-amp-hr}} \times E(I)\ \text{volts} \times \frac{1\ \text{amp}}{1000\ \text{ma}} \times I\ \frac{\text{ma}}{\text{cm}^2}$$

$$= 0.8604\ I \times E(I)$$

where $E(I)$ is the working voltage of the cell, a function of current density.

Making an enthalpy balance, dividing by 1.865×10^{-5} I, and using the water balance to simplify

$$10.53\,(t_{in} - 18)F + \left[12.15(t_{in} - 18) - 86{,}702.\right] \frac{p(0,\, t_{in})}{(P - p(0, t_{in})}(F-1)$$

$$= \quad 10.53\,(t_{out} - 18) + \left[12.15(t_{out} - 18) - 86{,}702\right] \frac{p(N,\, t_{out})}{P - p(N,\, t_{out})}\,(F-1)$$

$$+ 46{,}134.\ E(I)$$

which holds for any $I > 0$

Solving for t_{out}

$$t_{out} = 18 + \frac{(t_{in} - 18)\left\{10.53F + 12.15\,\dfrac{p(0,\, t_{in})}{P - p(0,\, t_{in}}\,(F-1)\right\}}{\left[10.53 + 12.15\left(\dfrac{p(N,\, t_{out})}{P - p(N,\, t_{out})}\right)\right](F-1)}$$

$$+ \frac{57{,}801 - 46{,}134.\ E(I)}{\text{same denominator}} \qquad (2)$$

For a particular cell we require the polarization curve, E(I) As an example, an empirical correlation gives

$$E(I) = 1.045 - 1.25 \times 10^{-4}\, I - 0.052 I^{0.250};\ 0 \le I \le 200 \qquad (3)$$

for a cell with standard AB-1 electrodes and "ACCO" asbestos matrix, operating at 70°C.

For a particular electrolyte we also require the vapor pressure of water as a function of temperature and normality. For KOH solutions, empirical correlation of data from I.C.T. 3, p. 373 gives:

$$p(N, t) = \begin{bmatrix} 1 - C_1 N - C_2 N^2;\ N < 6 \\ C_3 - C_4 N - C_5 N^2;\ N > 6 \end{bmatrix} \times 10^{\left\{C_6 + C_7 \log_{10} \frac{t + 273.18}{100} + \left(\frac{C_8}{\frac{t + 273.18}{100}}\right)\right\}}; \qquad (4)$$

$50 \le t \le 120;\ 0 \le N \le 13$

$C_1 = 0.0350$ $\quad C_5 = -0.001685$

$C_2 = 0.003415$ $\quad C_6 = 9.94606$

$C_3 = 1.1836$ $\quad C_7 = -4.13306$

$C_4 = 0.0962$ $\quad C_8 = -28.295$

Finally, we need the inverse of Equation (4); given p(n,t) and t we compute N as

$$\left.\begin{aligned} N_L &= -\frac{C_1}{2C_2} + \sqrt{\left(\frac{C_1}{2C_2}\right)^2 + \left\{1 - \frac{p(N,t)}{\phi}\right\} \Big/ C_2} \\ N_H &= -\frac{C_4}{2C_5} + \sqrt{\left(\frac{C_4}{2C_5}\right)^2 + \left\{C_3 - \frac{p(N,t)}{\phi}\right\} \Big/ C_5} \\ \phi &= 10^{\left\{C_5 + C_6 \,\mathrm{LOG}\left(\frac{t+273.18}{100}\right) + \frac{C_7}{\left(\frac{t+273.18}{100}\right)}\right\}} \end{aligned}\right\} \qquad (5)$$

$$N = \begin{cases} N_L, & \text{if } \quad 0 \le N_L \le 6 \\ N_H, & \text{if } \quad 13 \ge N_H > 6 \end{cases}$$

otherwise N cannot be determined.

COMPUTATION SCHEME

For a particular set of parameters (P, t_{in}, F, I):

(i) Equations (4) and (1) are solved for $p(N,t_{out})$

(ii) Equations (2), (3), (4) are solved for t_{out})

(iii) Equation (5) is solved for N

Note that all computations are explicit (no iteration is required).

Sample calculation

Parameters: $I = 100.\ ma/cm^2$,

$F = 15.$

$t_{in} = 94.6°C$

$P = 1.\ atm$

Basic results: $p_{in} = 0.82223\ atm$

$p_{out} = 0.82372\ atm$

$t_{out} = 113.64°C$

$N_{cell} = 8.083$

REFERENCES

(1) "Research and Development of High-Performance Light-Weight Fuel Cell Electrodes", American Cyanamid Company, First Quarterly Report, Nov. 1, 1963 to Jan. 31, 1964, NASA CR-54022.

(2) "Power Transformation and Voltage Regulation - A Report on Contract Programs NOW 60-0824c and NOW 62-0984d at General Electric Co." Proceedings of Symposium held in Washington D. C. on July 18, 1963.

DISTRIBUTION LIST FOR SECOND QUARTERLY REPORT

National Aeronautics & Space Administration
Washington, D. C. 20546

Attention:	Miss Millie Ruda, Code AFSS-LD	3
Attention:	Walter L. Scott, Code RPP	1
Attention:	Ernst M. Cohn, Code RPP	1
Attention:	George E. Esenwein, Code MSA	1
Attention:	H. B. Finger, Code RP	1
Attention:	A. M. Andrus, Code FC	1
Attention:	J. R. Miles, Code SL	1
Attention:	Fred Schulman, Code RN	1

National Aeronautics & Space Administration
Goddard Space Flight Center
Greenbelt, Maryland

Attention:	Thomas Hennigan	1

National Aeronautics & Space Administration
Lewis Research Center
21000 Brookpark Road
Cleveland, Ohio 44135

Attention:	B. Lubarsky, MS 86-1	1
Attention:	N. D. Sanders, MS 302-1	1
Attention:	N. T. Musial, MS 77-1	1
Attention:	M. J. Sarri, MS 86-1	1
Attention:	R. L. Cummings, MS 86-1	1
Attention:	H. J. Schwartz, MS 86-1	1
Attention:	John E. Dilley, MS 86-1	1
Attention:	W. A. Robertson, MS 86-1	1 + 1 repro.

National Aeronautics & Space Administration
Marshall Space Flight Center
Huntsville, Alabama

Attention:	Philip Youngblood	1
Attention:	Eugene Cagle	1

National Aeronautics & Space Administration
Manned Space Craft Center
Houston 1, Texas

Attention:	W. R. Dusenbury Systems Evaluation & Development Div. Rich Building 6040 Telephone Road	1
Attention:	Robert Cohen Gemini Project Office	1

National Aeronautics & Space Administration
Scientific and Technical Information Facility
P. O. Box 5700
Bethesda, Maryland

Attention:	NASA Representative	2 + 1 repro.

National Aeronautics & Space Administration
Western Operations Office
150 Pico Boulevard
Santa Monica, California
Attention: P. Pomerantz 1

Jet Propulsion Laboratory
4800 Oak Grove Drive
Pasadena, California
Attention: Aiji Uchiyama 1

U. S. Army Engineer R & D Labs
Fort Belvoir, Virginia
Attention: B. C. Almaula, 1
Electrical Power Branch

U. S. Army Electronics R. & D Labs
Fort Monmouth, New Jersey
Attention: David Linden, Code SELRA/SL-PS 1
Attention: Dr. Adolph Fischbach, Code SELRA/SL-PS 1

U. S. Army R & D Liaison Group (9851 DN)
APO 757
New York, New York
Attention: Chief, Chemistry Branch 1

U. S. Army Research Office
Physical Sciences Division
3045 Columbia Pike
Arlington, Virginia
Attention: Dr. Sidney J. Magram 1

Harry Diamond Labs
Room 300, Building 92
Connecticut Avenue & Van Ness Street, N. W.
Washington, D. C.
Attention: Robert Goodrich 1

Army Material Command
Research Division
AMCRD-RSCM T-7
Washington 25, D. C.
Attention: John W. Crellin 1

U. S. Army Trecom
Physical Sciences Group
Fort Eustis, Virginia
Attention: Dr. R. L. Echols (SMOFE-PSG) 1

(Continued - Distribution List)

U. S. Army Research Office
Box CM, Duke Station
Durham, North Carolina
Attention: Dr. Wilhelm Jorgensen 1

U. S. Army Mobility Command
Research Division
Center Line, Michigan
Attention: O. Renius (AMSMO-RR) 1

Headquarters, U. S. Army Material Command
Development Division
Washington 25, D. C.
Attention: Marshall D. Aiken (AMCRD-DE-MO-P) 1

Research Office
R & D Directorate
Army Weapons Command
Rock Island, Illinois
Attention: G. Reinsmith, Chief 1

Office of Naval Research
Department of the Navy
Washington 25, D. C.
Attention: Dr. Ralph Roberts 1
Attention: Dr. J. C. White 1

Bureau of Naval Weapons
Department of the Navy
Washington 25, D. C.
Attention: Whitwell T. Beatson (Code RAAE-52) 1

Bureau of Ships
Department of the Navy
Washington, D. C.
Attention: Bernard B. Rosenbaum, Code 340 1
Attention: C. R. Viglotti, Code 660 1

Naval Ordnance Laboratory
Department of the Navy
Corona, California
Attention: Mr. W. C. Spindler 1

Naval Ordnance Laboratory
Department of the Navy
Silver Springs, Maryland
Attention: P. B. Cole, Code WB 1

Wright-Patterson AFB
Aeronautical Systems Division
Dayton, Ohio
Attention: R. L. Kerr 1
Attention: J. E. Cooper 1

AF Cambridge Research Lab
Attn. CRZE
L. G. Hanscom Field
Bedford, Massachusetts
Attention: F. X. Doherty 1
Attention: Edward Raskind (Wing F) 1

Rome Air Development Center, ESD
Griffiss AFB, New York
Attention: F. J. Mollura (RASSM) 1

Headquarters, USAF (AFRST-PM)
Washington, D. C.
Attention: Lt. Col. W. G. Alexander 1

Space Systems Division
Attention: SSZAE-11
Air Force Unit Post Office
Los Angeles 45, California
Attention: Captain W. H. Ritchie 1

Air Force Ballistic Missile Division
Attn. WEZYA-21
Air Force Unit Post Office
Los Angeles 45, California
Attention: Captain William Hoover 1

Advanced Research Projects Agency
The Pentagon
Washington, D. C.
Attention: C. F. Yost, Room 3E 153 1
Asst. Director, Material Sciences
Attention: Dr. J. H. Huth, Room 3E 157 1

U. S. Atomic Energy Commission
Auxiliary Power Branch (SNAP)
Division of Reactor Development
Washington, D. C. 1

U. S. Atomic Energy Commission
Division of Reactor Development
Advanced Space Reactor Branch
Washington, D. C.
Attention: Lt. Col. J. H. Anderson 1

(Continued - Distribution List)

U. S. Atomic Energy Commission
Army Reactors DRD
Washington, D. C.
Attention: D. B. Hoatson 1

Defense Documentation Center Headquarters
Cameron Station, Building 5
5010 Duke Street
Alexandria 4, Virginia
Attention: TISIA 1

Office DDR&E USW & BSS
The Pentagon
Washington, D. C.
Attention: G. B. Wareham 1

Institute for Defense Analyses
Research and Engineering Support Division
1666 Connecticut Avenue, N. W.
Washington 9, D. C.
Attention: Dr. G. C. Szego 1

Power Information Center
University of Pennsylvania
Moore School Building
200 South 33rd Street
Philadelphia 4, Pennsylvania 1

Office of Technical Services
Department of Commerce
Washington 25, D. C. 20009 1

Alfred University
Alfred, New York
Attention: Professor T. J. Gray 1

Allis-Chalmers Manufacturing Company
1100 S. 70th Street
Milwaukee 1, Wisconsin
Attention: Dr. T. G. Kirkland 1

Allison Division of General Motors
Indianapolis 6, Indiana
Attention: Dr. R. E. Henderson 1

American Machine & Foundry
689 Hope Street
Springdale, Connecticut
Attention: Dr. L. H. Shaffer
Research & Development Division 1

Astropower, Incorporated
2968 Randolph Avenue
Costa Mesa, California
Attention: Dr. Carl Berger 1

Battelle Memorial Institute
Columbus 1, Ohio
Attention: Dr. C. L. Faust 1

Bell Telephone Laboratories, Incorporated
Murray Hill, New Jersey
Attention: U. B. Thomas 1

Clevite Corporation
Mechanical Research Division
540 East 105th Street
Cleveland, Ohio
Attention: A. D. Schwope 1

Electrochemica Corporation
1140 O'Brien Drive
Menlo Park, California
Attention: Dr. Morris Eisenberg 1

Electro Optical Systems, Incorporated
300 N. Halstead
Pasadena, California
Attention: E. Findl 1

Engelhard Industries, Incorporated
497 Delancy Street
Newark 5, New Jersey
Attention: Dr. J. G. Cohn 1

Esso Research and Engineering Company
Products Research Division
P. O. Box 215
Linden, New Jersey
Attention: Dr. Carl Heath 1

The Franklin Institute
Philadelphia, Pennsylvania
Attention: Mr. Robert Goodman 1

Fuel Cell Corporation
5717 Elward Avenue
St. Louis 20, Missouri 63210
Attention: Mr. S. S. Adams 1

General Electric Company
Direct Energy Conversion Operations
Lynn, Massachusetts
Attention: Dr. E. Glazier 1

(Continued - Distribution List)

General Electric Company
Research Laboratory
Schenectady, New York
Attention: Dr. H. Liebhafsky 1

General Motors Corporation
Box T
Santa Barbara, California
Attention: Dr. C. R. Russell 1

Hoffman Electronics Company
Research Laboratory
Santa Barbara, California
Attention: Dr. J. Smatko 1

Leesona Moos Laboratories
Lake Success Park
Community Drive
Great Neck, New York
Attention: Dr. A. Moos 1

McDonnell Aircraft Corporation
P. O. Box 516
St. Louis 66, Missouri
Attention: Project Gemini Office 1

Monsanto Research Corporation
Boston Laboratories
Everett 49, Massachusetts
Attention: Dr. J. O. Smith 1

North American Aviation Company
S & ID Division
Downey, California
Attention: Dr. James Nash 1

Pratt and Whitney Aircraft Division
United Aircraft Corporation
East Hartford 8, Connecticut Attention: Librarian

Radio Corporation of America
Astro Division
Heightstown, New Jersey
Attention: Dr. Seymour Winkler 1

Speer Carbon Company
Research and Development Laboratories
Packard Road at 47th Street
Niagara Falls, New York
Attention: Dr. L. M. Liggett 1

(Continue - Distribution List)

Thiokol Chemical Corporation
Reaction Motors Division
Denville, New Jersey
Attention: Dr. D. J. Mann 1

Thompson Ramo Wooldridge
23555 Euclid Avenue
Cleveland 17, Ohio
Attention: Librarian 1

Union Carbide Corporation
Technical Information Service
P. O. Box 6116
Cleveland, Ohio 44101

University of California
Space Science Laboratory
Berkeley 4, California
Attention: Prof. Charles W. Tobias 1

University of Pennsylvania
Electrochemistry Laboratory
Philadelphia 4, Pennsylvania
Attention: John O'M. Bockris 1

Western Reserve University
Cleveland, Ohio
Attention: Prof. Ernest Yeager 1